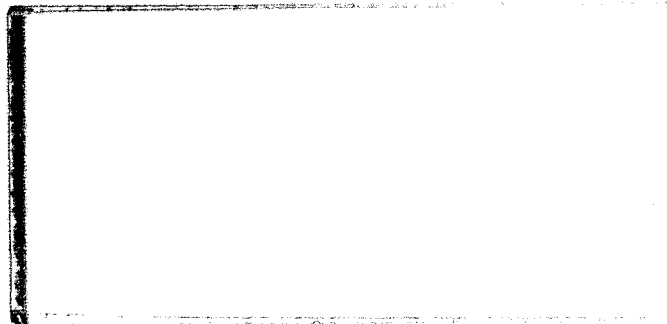


## N O T I C E

THIS DOCUMENT HAS BEEN REPRODUCED FROM  
MICROFICHE. ALTHOUGH IT IS RECOGNIZED THAT  
CERTAIN PORTIONS ARE ILLEGIBLE, IT IS BEING RELEASED  
IN THE INTEREST OF MAKING AVAILABLE AS MUCH  
INFORMATION AS POSSIBLE



(NASA-CR-163918) THE LOCKHEED OSO-8  
PROGRAM. TASK 2: ANALYSIS OF DATA FROM THE  
HIGH RESOLUTION ULTRAVIOLET SPECTROMETER  
EXPERIMENT Final Report, 19 Nov. 1977 - 31  
Aug. 1980 (Lockheed Missiles and Space Co.) G3/92

N81-16966

Unclas  
43554



# LOCKHEED

MISSILES & SPACE COMPANY, INC. • SUNNYVALE, CALIFORNIA

THE LOCKHEED OSO-8 PROGRAM

FINAL REPORT

Task II: Analysis of Data from the  
High Resolution Ultraviolet  
Spectrometer Experiment

E.C. Bruner, Jr.

THE LOCKHEED OSO-8 PROGRAM

Analysis of Data from the High Resolution Ultraviolet  
Spectrometer Experiment

Dr. E.C. Bruner, Jr.

Lockheed Palo Alto Research Laboratory  
Department 52-i2, Building 202  
3251 Hanover Street  
Palo Alto, California 94304

30 September 1980

Final Report for the Period 19 November 1977 - 31 August 1980

Prepared for

GODDARD SPACE FLIGHT CENTER  
Greenbelt, Maryland 20771

TECHNICAL REPORT STANDARD TITLE PAGE

1. Report No.		2. Government Accession No.		3. Recipient's Catalog No.	
4. Title and Subtitle THE LOCKHEED OSO-8 PROGRAM Analysis of Data from the High Resolution Ultraviolet Spectrometer Experiment				5. Report Date 30 September 1980	
				6. Performing Organization Code	
7. Author(s) E.C. Bruner, Jr.				8. Performing Organization Report No. LMSC/D766867	
9. Performing Organization Name and Address Lockheed Palo Alto Research Laboratory Dept. 52-12, Bldg. 202 3251 Hanover Street Palo Alto, California 94304				10. Work Unit No.	
				11. Contract or Grant No. NAS5-22411 Task II	
12. Sponsoring Agency Name and Address NASA Goddard Space Flight Center Greenbelt, Maryland 20771				13. Type of Report and Period Covered Final (Type III) - Nov. 19, 1977 - Aug. 31, 1980	
				14. Sponsoring Agency Code	
15. Supplementary Notes					
16. Abstract  The complete set of C IV time sequences generated by the University of Colorado high resolution ultraviolet spectrometer experiment on OSO-8 have been examined in a comprehensive and systematic fashion. As a result a new limit is placed on the acoustic flux passing through the transition zone of the sun's atmosphere. It is found to be three orders of magnitude too small to heat the corona, and is consistent with zero. In collaborative efforts, the properties of transient C IV brightenings have also been examined in considerable detail.					
17. Key Words (Selected by Author(s)) OSO-8 / ultraviolet spectrometer/ C IV time series			18. Distribution Statement		
19. Security Classif. (of this report) Unclassified		20. Security Classif. (of this page) Unclassified		21. No. of Pages 78	22. Price*

\*For sale by the Clearinghouse for Federal Scientific and Technical Information, Springfield, Virginia 22151.

## PREFACE

The present report describes activities undertaken as part of NAS5-22411 Task II. The objective of this portion of the contract was to analyze a specific set of solar data generated by the University of Colorado high resolution ultraviolet spectrometer experiment on OSO-8, and to report the results therefrom. The success with which this objective has been met is reflected in the production of the three articles referred to in the text, one of which has already appeared in print, and the other two of which are in press. The results of these studies are summarized, and pre-publication versions of the latter two articles provided in Appendicies B and C.

## TABLE OF CONTENTS

	Page
1. Introduction.....	1
2. Scope of Data.....	1
3. Software Development and Documentation.....	2
4. Extent of Data Analysis.....	4
5. Dissemination of Reduced Data.....	4
6. Principal Scientific Results.....	4
7. New Technology.....	6
Appendix A: Publications and Presentation of the Ultraviolet Spectrometer Data Analysis Program.....	7
Appendix B: "OSO-8 Observations of the Impulsive Phase of Solar Flares in the Transition-Zone and Corona".....	8
Appendix C: "OSO-8 Observational Limits to the Acoustic Coronal Heating Mechanism".....	47
Bibliography.....	73
Index.....	74

## 1. INTRODUCTION

The following report summarizes a portion of the work performed under Contract NAS5-22411, as dictated by the guidelines contained therein.

Contract NAS5-22411 included the obligation to perform three major tasks:

- (a) orbital operations of the Lockheed Mapping X-Ray Heliometer experiment on OSO-8 (Task Ia)
- (b) the analysis and dissemination of data therefrom (Task Ib)
- and (c) the analysis of data from the University of Colorado high resolution ultraviolet spectrometer experiment on OSO-8 (Task II).

The results of Task Ia have been previously reported (Wolfson, Acton, and Smith, 1978)\*, and those of Task Ib are being described in a concurrent report (Acton et al., 1980). The present report therefore confines itself to the activities undertaken under Task II.

Details of the University of Colorado experiment will be found in Bruner (1977), and in the publications of the Laboratory for Atmospheric and Space Physics listed in the bibliography to this report.

## 2. SCOPE OF DATA

The high resolution ultraviolet spectrometer experiment gathered a large volume of data at a variety of wavelengths and in a variety of observing modes, both stationary and spectroheliographic, as described by Hansen and Bruner (1979). The portion of this larger data set falling within the scope of the present analysis effort consists of two parts:

- (a) time series of repetitive scans of the C IV 1548A line made with the spectrograph slit in a fixed position.
- (b) time series of repetitive scans of the Si IV 1393A line made with the spectrograph slit in a fixed position.

Both of these are transition-zone lines, the latter being thought to be formed somewhat lower than the former. Copies of all observing runs performed in these two modes are available at Lockheed on magnetic tape. In the case of the C IV time series, this consists of approximately 300 orbits spread over a period of 15 months. In the case of the Si IV time series, approximately 60 orbits are involved.

\*(publications developed under this contract are listed in Appendix A; all other references are listed in the Bibliography).

### 3. SOFTWARE DEVELOPMENT AND DOCUMENTATION

The relevant data tapes were reformatted and documented at the University of Colorado using the procedures described by Hansen and Bruner (1979). A series of additional software programs were developed at Lockheed to perform the specific tasks required for the present analysis. These programs make use of the SOL language, which was specially created at the University of Colorado for the manipulation of the reformatted data (Stern and Klemp, 1976). The following functions are available:

- (a) Plot raw data, i.e., the repetitive scans of line profiles.
- (b) Remove long-term trends by polynomial fit, thereby removing effects of orbital motion and detector shift.
- (c) Compute moments of each line profile, thereby obtaining discrete time series of intensity and velocity.
- (d) Compute root-mean-square of intensity and velocity fluctuations for each time series.
- (e) Compute and display power spectra of intensity and velocity.
- (f) Compute and display cross correlation of velocity and intensity fluctuations with variable time delay.
- (g) Compute and display estimated contributions to the acoustic energy flux.
- (h) Compute noise contributions to velocity field for statistically-perturbed model intensities.

Programs (a) - (g) were developed and executed on a PDP 11/34 minicomputer with hardcopy capability. Program (h) was developed on a Commodore 2001 "home" computer purchased by the author for that purpose.

Figure 3.1 provides an example of some of the software capabilities as applied to a typical orbit of "raw" data. Additional examples may be found in Appendices B and C, and in the cited references.



#### 4. EXTEND OF DATA ANALYSIS

##### 4.1 Carbon IV Data

All 300 orbits of C IV time sequences have been examined in detail. The line profile sequence of each has been extracted, and hardcopies of same preserved and catalogued in a series of notebooks. For most, the intensities, velocities, power spectra and cross-correlations have also been produced. These are likewise preserved in the archival notebooks.

##### 4.2 Silicon IV Data

Only a portion of the Si IV data has yet been examined. A proposal has been accepted to examine these data in greater depth in a follow-on contract, NAS5-25906.

#### 5. DISSEMINATION OF REDUCED DATA

The primary responsibility for the dissemination of reduced data from the high resolution ultraviolet spectrometer experiment lies with the University of Colorado. The present contract carries no additional obligation in this regard, aside from the normal publication and presentation of scientific results which is dealt with in the next section and in Appendices A through C.

#### 6. PRINCIPAL SCIENTIFIC RESULTS

The principal scientific results obtained during the course of the present analysis of Carbon IV time series are fully described in the publications given in Appendix A. Pre-publication versions of those still in press are provided in Appendices B and C. The following is a summary of their conclusions.

##### 6.1 Transient Phenomena in the Transition Zone

In a preliminary study by Bruner and Lites (1979), the characteristics of 20 short-lived brightenings observed by the high resolution ultraviolet spectrometer in C IV were examined. During the period of the present contract, this study has been extended, primarily through the efforts of collaborators at the University of Colorado, to include: (a) all available

short-lived brightenings in C IV (Sec. 6.1.1), and (b) four major flare events having simultaneous coverage in H-alpha, X-rays, and microwaves (Sec. 6.1.2).

#### 6.1.1 Short-Lived Ultraviolet Brightenings

The results of the comprehensive study of short-lived C IV brightenings are presented in the article by Athay, White, Lites, and Bruner (1980). The events referred to appear to be common features of the transition zone atmosphere overlying normal solar active regions. For a typical large region, they occur with a frequency of about 3 per minute (only a fraction of which are seen by the spectrometer experiment because of its field of view), and involve brightenings on the order of a factor of 4 which persist over periods lasting anywhere from the resolution limit of 30 seconds up to 5 minutes or more. In the preliminary study, a strong association was found with red-shifts (i.e., with downward moving material) and a shock wave mechanism suggested as a plausible mode of production. The new comprehensive study leans towards the interpretation of the brightenings as being density enhancements associated with the streaming of prominence-like material, the red-shifted components being the analogue of coronal rain, and the blue shifted components that of surges.

#### 6.1.2 Flares

The new C IV flare study published by Lites, Bruner, and Wolfson (1980, Appendix B) draws not only upon the ultraviolet spectrometer time sequences, but also upon simultaneous X-ray and ground-based H-alpha and microwave observations (the X-ray effort having been handled under Task Ib of this same contract). Four events were studied in detail: one from March, 1976, and the remaining three from April, 1978. The present results have re-emphasized the importance of the indications of mass motion discovered in the preliminary study. Red shifts of 80 km/sec and more are observed in the early stages of these larger flares. This dynamic instability of the transition-zone atmosphere is often found to precede the more or less simultaneous onset of brightening at all wavelengths. The X-ray intensity is found to peak after the peak of the C IV brightness, and to be preceded by a shift from downflows to somewhat weaker upflows in the transition-zone. This blue shifted component at the level of C IV is interpreted as representing an evaporation of chromospheric material which by filling the coronal loops provides a basis for the soft X-ray emission

## 6.2 The Acoustic Flux in the Transition Zone

Notwithstanding the preceding projects, the primary focus of scientific activity under the present contract has been on the effort to place an improved limit on the possible intensity of the flux of acoustic energy passing through the transition zone and its relevance to coronal heating. This work is essentially an extension of the preliminary study by Bruner (1978), and the new results are reported in Bruner (1980, Appendix C).

The new study improves on the earlier one by incorporating explicitly the effects of photon statistics which can create the appearance of large spurious acoustic flux in areas of low intensity, and also by making a sharper distinction between the upward-propagating, downward-propagating, and evanescent components of the observed "waves". Upward and downward-directed components were found in roughly equal numbers. When the noise component is removed, the limit on the possible net upward flux is found to be three orders of magnitude below that which would be required to heat the corona.

## 7. NEW TECHNOLOGY

Due to the nature of the work, no new technology was developed during the course of this effort.

PUBLICATIONS AND PRESENTATIONS OF THE  
LOCKHEED OSO-8 ULTRAVIOLET SPECTROMETER DATA ANALYSIS PROGRAM

I. Primary Publications of Scientific Results

Bruner, E.C., Jr. (1980): "OSO-8 Observational Limits to the Acoustic Coronal Heating Mechanism", accepted for publication in The Astrophysical Journal.

II. Collaborative Publications

Athay, R.G., White, O.R., Lites, B.W., and Bruner, E.C., Jr. (1980): "Impulsive EUV Bursts Observed in C IV with OSO-8", Solar Physics, 66, pp. 357-370.

Lites, B.W., Bruner, E.C., Jr., and Wolfson, C.J. (1980): "OSO-8 Observations of the Impulsive Phase of Solar Flares in the Transition-Zone and Corona," accepted for publication in Solar Physics.

III. Brief or Informal Reports and Presentations

Lites, B.W., Bruner, E.C., and Hansen, E.R., "OSO-8 Measurements of Rapid Downflow in the Transition Zone During the Impulsive Phase of Solar Flares", presented at the American Astronomical Society Meeting, 26-28 June 1978. Abstract: Bull. A.A.S., 10, 441.

Bruner, E.C., Jr., "Experimental Search for Sound Waves in the Transition Zone," presented at a University of Hawaii Colloquium, May 1979.

Bruner, E.C., Jr., "OSO-8 Observational Limits to the Acoustic Coronal Heating Mechanism," presented at the American Astronomical Society Meeting 13-18 January, 1980. Abstract: Bull. A.A.S., 11, 697.

OSO-8 OBSERVATIONS OF THE IMPULSIVE PHASE OF SOLAR FLARES  
IN THE TRANSITION-ZONE AND CORONA

Bruce W. Lites, E.C. Bruner, Jr., and  
C.J. Wolfson

Accepted for publication in Solar Physics

OSO-8 OBSERVATIONS OF THE IMPULSIVE PHASE OF  
SOLAR FLARES IN THE TRANSITION-ZONE AND CORONA

Bruce W. Lites\*

Laboratory for Atmospheric and Space Physics  
University of Colorado at Boulder

E. C. Bruner, Jr. and C. J. Wolfson  
Lockheed Palo Alto Research Laboratory  
Palo Alto, California

\*Currently at: High Altitude Observatory  
National Center for Atmospheric Research  
P.O. Box 3000  
Boulder, Colorado 80307

## ABSTRACT

Several solar flares have been observed from their onset in C IV  $\lambda 1548.2$  and 1-8 Å x-rays using instruments aboard OSO-8. In addition, microwave and H $\alpha$  flare patrol data have been obtained for this study. The impulsive brightening in C IV is frequently accompanied by redshifts, interpreted as downflows, of the order of 80 km s<sup>-1</sup>. The maximum soft x-ray intensity usually arrives several minutes after the maximum C IV intensity. The most energetic C IV event studied shows a small blueshift just before reaching maximum intensity, and estimates of the mass flux associated with this upflow through the transition-zone are consistent with the increase of mass in the coronal loops as observed in soft x-rays. This event had no observable microwave burst, suggesting that electron beams did not play a major role in the chromospheric and transition-zone excitation. Lastly, our observations suggest that the frequent occurrence of violent dynamical processes at the onset of the flare are associated with the initial energy release mechanism.

## INTRODUCTION

In a previous paper (Bruner and Lites 1979, hereafter referred to as Paper I) we reported on impulsive flare-like brightenings of the transition-zone over active regions which were frequently accompanied by redshifts measured in the C IV 1548 Å line. The measurements used in Paper I were all taken during the first nine months of the OSO-8 mission when solar activity was at a very low level. During most of the next 18 months, solar activity remained low, and the sensitivity of the University of Colorado (CU) instrument at 1548 Å and blueward declined to a level such as to render it essentially useless at these wavelengths. For reasons still not fully understood, near the end of 1977, the instrument recovered much of its earlier short wavelength sensitivity. This renewed sensitivity allowed us to resume our observational program to study the dynamical state of the transition-zone in solar flare events.

In this paper we report on observations of small solar flares occurring during the period of intense solar activity in April and May of 1978. These observations are unique in that the flares are observed from their onset. Some of the events are much more energetic than those reported in Paper I, and the observations indicate that they may result from a different physical mechanism than that proposed for the original set of events. We have selected several of the more energetic of these events for detailed study, with the intent of using all available

data on these events to understand the relationship of the dynamical processes in the transition-zone to the manifestation of the flares in the corona and chromosphere.

## OBSERVATIONS

In addition to OSO-8 observations of the C IV line, we bring together observations of the soft x-ray emission as monitored by the Lockheed Mapping X-ray Heliometer on-board OSO-8, ground-based H $\alpha$  flare patrol films, and solar microwave radio emission. Of the more than 30 events observed, we have selected four events that were well-observed by OSO-8 in both x-rays and the ultraviolet. Table I summarizes these four events.

Bruner (1977) give a description of the University of Colorado ultraviolet spectrometer aboard OSO-8. We monitor the development of the transition zone flare and its dynamical state in the same manner as discussed in Paper I; i.e., we repeatedly scan the line profile of the C IV 1548.2 Å line from blue to red. We cover a 0.75 Å range about the line center with a wavelength sampling interval at 0.075 Å. The experiment repeats the scan at intervals of either 49.5 or 27.5 seconds. We used the shorter scan time for some of the later events because the high intensities observed in the earlier events indicated that better time resolution could be had with little loss in the quality of the observed flare profiles. Most of the events were recorded at the location in the active region of maximum preflare brightness of the C IV line. This was accomplished by preceding the series of line profile scans by an emission (EMAX) maximum experiment: a raster scan over the active region which selects the most intense location and instructs the spacecraft to point at this position during the following experiment.

Examination of these EMAX rasters has shown that the brightest area of the active region in CIV was located in the adjacent plage, not over the sunspot. We have found through examination of many orbits of data throughout the 3-year OSO-8 mission that the sunspots are very seldom the brightest features of active regions seen in CIV. On the other hand, Foukal, et al. (1974) have shown that many transition-zone lines were very bright over two sunspots. We offer the following possibilities to explain the difference between our results, and the result of Foukal, et al. First, our raster element size is either 10 x 20 or 20 x 20 arc seconds, or 8 to 16 times the element size of Foukal, et al. The bright features in the sunspot are quite small in CIII in their images, and these features may not be much larger in CIV. This indicates that the average intensity over our raster element size may not compete with the plage intensity. Secondly, sunspot observations of the CIV line with a 2 x 20 arc second resolution (Lites, 1980) show a sunspot umbra to be fainter than a nearby plage by a factor of 3. Thirdly, low excitation lines (those formed below  $10^{50}$ K) in the Foukal, et al. data are not greatly enhanced over a sunspot. CIV is formed somewhat below  $10^{50}$ K at quiet sun densities, and tends to be formed at lower temperatures as the density increases (Lites, et al. 1980). For these reasons, along with our raster images from the EMAX experiments which allow us to locate our slit within the active region, we can demonstrate in each case that the slit was located over bright plage regions.

The Lockheed Mapping X-ray Heliometer (MXRH) is sensitive to x-rays with energies from 1.5 - 15 keV and obtains spectral information by 14 channel pulse height analysis of its six proportional counter detector outputs. It has an angular resolution of about 2 minutes of arc and can thereby isolate single active regions, but cannot examine a spatial detail within an active region. The MXRH has a temporal resolution of about 20 s. A more complete description of MXRH observations may be found in Wolfson et al. (1977); instrumental details are given by Wolfson et al. (1975). The temperatures and emission measures presented in Table I for the x-ray emitting plasma were obtained under the simplifying assumption that, after the preflare (i.e., active region) contribution is removed from the total emission, the remainder may be considered isothermal. The parameters of the resultant flare plasma were then determined, on a best fit basis, by folding theoretical x-ray spectra (similar to those of Tucker and Koren (1971)) through the MXRH instrument response.

The first event of Table 1 is also listed in Paper I, and we discuss this event in detail since it seems to belong in the class of the more energetic events, and it has good  $H_{\alpha}$  and x-ray coverage. Unlike the remainder of the events, Event 1 was measured in the penumbra of a sunspot. Events 2, 3, and 4 are also very energetic transition-zone events associated with  $H_{\alpha}$  sub-flares or flares. The various sources of the  $H_{\alpha}$  coverage of these events are given in Table I, along with several observational parameters of the events in the C IV line, and x-rays. The rise time listed in Table I is the duration of the impulsive

brightening phase of the C IV emission. The flare to preflare brightness ratio ( $I/I_0$ ) given in Table I is the ratio of the maximum C IV brightness at line center during the event to the preflare line center intensity. The C IV line broadens drastically in most of the events and thus makes a determination of the background intensity difficult with our 0.75 Å range. We have nonetheless made an extrapolation of the line wings to obtain the time history of the background intensity. The maximum enhancement of the background intensity,  $I/I_0$  (background) in Table I, is the result of this estimate. The velocities listed in the table result from an estimate of the maximum displacement of the new energy in the C IV line during the impulsive rise in intensity.

Dr. S. Enome has kindly provided us with the history of the solar microwave emission as recorded at the Toyokawa Observatory at frequencies from 1000 to 9400 MHz for events 2, 3, and 4. Event 2 shows no apparent microwave burst, hence we do not plot the microwave emission in Figure 2. Figures 1 - 4 show the time evolution of the flare intensities in C IV, soft x-rays, and microwaves at 3750 MHz. In the following, we discuss some of the observational implications of the time history of these events.

## DYNAMICS OF THE C IV EMITTING REGION

Table I indicates that there are considerable mass motions associated with the onset of the flare brightenings in the transition-zone. Line shifts and intensities are determined in the manner described in Paper I. The largest line shifts are towards the red, and occur just prior to the steepest rise in intensity. This result is in accordance with the findings of Paper I for smaller events. The evolution of the C IV profile for event 2 is given in detail in Figure 5, where a series of 20 line profiles are displayed. Unfortunately, there are two problems with these observations: a telemetry dump occurred during scan 11 and part of scan 12 causing us to permanently lose these data, and an error in the wavelength drive shifted the scan range after profile 16. Fortunately, both of these problems are well understood and do not severely hamper our understanding of the mass motions in this event. Redshifted material appears at profile 8, and reaches a maximum value of about  $90 \text{ km s}^{-1}$  at profile 10. Figure 5 shows a preflare average profile, and individual profiles 13 (redshifted material at  $65 \text{ km s}^{-1}$ ), and 14 (entire profile blueshifted by about  $10 \text{ km s}^{-1}$ ). The following two profile scans (15 and 16) are at the maximum intensity and the start of the declining phase of the event, respectively. They are nearly unshifted with respect to the preflare average profile.

In Paper I we discussed a spurious distortion of the line profile that could arise due to measurement of line profiles by the scanning techniques. The scanning process can introduce further distortion when both the line shape and background intensity vary by large amounts. We have substantially corrected for this problem using the interpolation procedure discussed in Paper I, and we find that the major profile distortions are solar in origin, not an artifact of our measurement process. This can be seen intuitively from Figure 5, where substantial redshifts develop and persist for several profiles before the intensity of either the background or the line rises by a large factor. In addition, the blueshift of profile 14 occurs while the intensity is still rising when the measurement process would introduce a redshift. By way of a cautionary note, however, we mention that we have observed changes in the C IV line center intensity on time scales as short as 3.5 seconds in other small flare-like events. Measurements of line profiles in flares should therefore be made on time scales an order of magnitude faster than we were capable of with OSO-8.

Events 1 and 3 show similar evidence for downward motions prior to and during the impulsive brightening in the transition zone, but neither of these events show a blueshift during the flare. The C IV line profile changed so rapidly during the impulsive brightening of event 4 that meaningful measurements of the mass flow during the initial phase of this event is not possible, even with the 27.5 second repeat time of each scan. Just after the time of maximum C IV intensity for event 4, the

line center is seen to be shifted to the red of the pre-event line center by about  $20 \text{ km s}^{-1}$ . This shift gradually returns to the pre-event value during the 15 minutes following the flare maximum.

Upon close inspection of the individual C IV profiles during all the flare events measured in April and May, 1978, one is struck with the impression that the transition-zone of the flaring region is dynamically unstable well before and after the onset of impulsive brightening. The line profiles frequently show both a dramatic distortion (most frequently to the red) and a broadening well before the impulse. Brueckner, et al. (1976) have seen similar instabilities prior to flare activity in active regions. This characteristic changeability of the profiles persists throughout the declining phase, and it may be related to the dynamic nature to the "steady" solar transition-zone (Athay and White, 1980) and entirely independent of the flare process. On the other hand, the flare process may be an energetic occurrence of this apparently continual instability of the transition-zone.

CORRESPONDENCE OF THE TRANSITION-ZONE EVENTS  
WITH THE LOW TEMPERATURE FLARE

Only a small fraction of the background intensity level measured by the CU OSO-8 instrument at wavelengths away from the C IV 1548.2 Å line is due to true spectral features at this wavelength. Scattered light in the spectrograph, generally thought to arise from the wavelength range 1700 to 1900 Å, dominates the background intensity. The background intensity level is therefore some measure of the conditions prevailing in the high photosphere and temperature minimum region of the atmosphere. Chipman (1978) used intensity fluctuations of this background with the intensity variations in several chromospheric and transition-zone lines to study wave propagation in the quiet solar atmosphere. Our repeated scans of the flaring C IV emission line contain this information as well, since in some cases the line profile is not precisely centered in the scan, so measurements are made far enough away from line center that little C IV line radiation is mixed in with the background intensity. This is true for event 4 of Table I. Table I gives the degree of brightening of the background in terms of the pre-event mean for each of the four events. We note that in all of these events except the first (recorded over a sunspot), substantial enhancement of the background occurred. To within the time resolution of the measurements, the impulsive brightening in the background parallels that of the C IV line.

In event 2 (shown in Figure 5) the enhancement of the background intensity is very strong and well-determined. If we assume that the background intensity is formed in LTE at a temperature of 4600 K, the observed brightening implies an increase in temperature of 700 K, or more, if the slit covers more area than the emitting region of the flare. This is a much greater increase than that found by Cook and Brueckner (1979), however, they use observations of flaring regions taken well after the impulsive phase of the flares, and they have no true pre-event spectrum with which to compare their flare observations. It is clear from figures 2 and 5 that the greatest enhancement of the background occurs before soft x-ray maximum in event 2. The maximum in soft x-ray flux occurs at about 23<sup>h</sup>35<sup>m</sup>, where the background intensity level, determined from the off-line-center scans of the C IV line, has fallen by a factor of 8 below its maximum value (coincident with the maximum in the C IV line). Significant heating of the temperature minimum region during flares has also been discussed recently by Machado, Emslie, and Brown (1978). A 700 K rise in temperature of this region is not unreasonable in view of their models of the flare atmosphere. It is important to point out that the scattered light contribution to the background intensity at 1548 Å is not due solely to continuum, but has a contribution from various chromospheric emission lines, notably Si III and Fe II, in the range 1700 to 1900 Å. Canfield, et al. (1978) have shown that the power radiated in the EUV continuum from 1400 to 1960 Å dominates that radiated in the lines by about a factor of 10 at the time of maximum emission

of the 5 September 1973 flare. We therefore feel confident in ascribing the flare-enhanced background radiation to enhancements near the temperature minimum, not to the chromosphere.

$H\alpha$  flare patrol images are of significant value to this study, since they allow us to visualize the response of the chromosphere to the flare energy release, and to estimate the fractional area of the OSO-8 CU slit covered by the flare. Figure 6 shows the development of event 1 in the  $H\alpha$  chromosphere. The  $H\alpha$  event commenced at nearly the same time as the C IV brightening, and we can see the event develop as a small, intense brightening at the edge of the sunspot and a more diffuse brightening at about 30 arcseconds from the edge of the sunspot. The OSO-8 CU slit was positioned across the brightening near the sunspot. The final two photographs in Figure 6 are taken off-band in  $H\alpha$ , and they demonstrate the possibility of redshifted (downflowing) material in the chromosphere near the time of flare maximum. The geometry of Figure 6 suggests that the  $H\alpha$  flare was confined to the footpoints of a magnetic flux loop with one end rooted in the sunspot.

Figure 7 presents a flare patrol image of event 2, with a superimposed orientation of the OSO-8 CU slit. The  $H\alpha$  sequence of photographs for event 2 shows brightening on- and off-band starting at about 23<sup>h</sup> 20<sup>m</sup> UT. Table I lists the fractional filling of the slit by  $H\alpha$  flare. Although we were not able to obtain actual photographs of events 3 and 4 in  $H\alpha$ , we estimate the slit filling factor from data given in the Solar-Geophysical Data. The effective areas of the chromospheric flares, also

given in Table I, are derived both from H $\alpha$  photographs and Solar-Geophysical Data. It appears that the chromospheric enhancement, as well as the enhancement at the temperature minimum in these events, starts at about the same time as the impulsive brightening in C IV.

COMPARISON OF THE TIME DEVELOPMENT OF THE FLARES  
IN THE TRANSITION-ZONE AND CORONA

In Figures 1-4 we present the time history of the flare soft x-ray emission along side of the development in the C IV line and microwaves at 3750 MHz for each of the events. From these four events (with the best observational coverage), and 7 others observed during the same period in both x-rays and C IV that are not discussed in this paper, a similar pattern seems to prevail. The following are general characteristics of the pattern:

1) The appearance of redshifted material in the transition-zone precedes by one or two minutes, or occurs simultaneously with, the rapid rise in soft x-rays. In event 3; however, the rise in x-rays starts about 30 seconds before the initial rise in C IV intensity. The MXRH views the entire flare area, whereas the CU instrument may sense only a small fraction of the flare. For this reason, an onset of flare brightening observed in C IV prior to the x-ray onset is significant, whereas the opposite case may not be significant, since the C IV events are quite energetic and hence are undoubtedly associated with detectable X-rays.

2) The C IV intensity always reaches a maximum before the soft x-rays. It appears that the initial rise in the transition-zone intensity approximately follows the derivative of the soft x-ray rise phase of the flare. To illustrate this property in Figure 8, we plot the differential of the x-ray flux along with the C IV intensity for events 2, 3, and 4. The time development of the derivative of the x-ray flux parallels the C IV intensity

during the rising phase very closely in events 2 and 4, while event 3 has already been mentioned as an exception to this rule.

3) The microwave bursts, when they occur, start at the same time as the brightening in the C IV line. The microwave bursts exhibit a more impulsive rise than either C IV or the soft x-rays. The relationship between the brightenings in the EUV and the soft x-ray and microwave bursts has been well observed previously (see Svestka 1976 for a review), but these events have significant dynamical processes in operation before the onset of the bulk of the coronal emission.

4) Two of the four events show a peak x-ray temperature during the impulsive rise in the transition-zone line, and well before the maximum in x-ray flux. This behavior has been noted by Datlowe, et al. (1974).

SOME PHYSICAL PROPERTIES OF THE FLARING REGIONS  
AS DERIVED FROM THE OBSERVATIONS

In Paper I, the brightenings in C IV were consistent with the physical picture of a shock front passing downward through the transition zone. This mechanism is probably not in force for the events that we report in this paper, for the degree of brightening is far too great for the velocities present. We are likely to be observing a situation where a certain volume of the chromosphere is being raised to transition-zone temperatures. In all of the C IV profiles observed in these 4 events, none shows a self-reversal, thus we infer that the lines are not extremely optically thick, and that the large increase in intensity results from a high density of the C IV plasma in the flare. If the C IV line does not have great optical depth, and if most of the emission comes from a temperature region close to the ionization peak of C IV, then Lites, Hansen and Shine (1979) demonstrated that the electron pressure  $P_e$  is given approximately by

$$P_e \approx 20 \frac{\bar{I}}{\tau_0} \frac{1}{V_T} \quad \text{dynes cm}^{-2} \quad (1)$$

where  $\bar{I}$  is the integrated C IV line intensity,  $\tau_0$  is the minimum line-center optical depth in any direction, and  $V_T$  is the total line broadening velocity (turbulent plus thermal). The above expression assumes a temperature of  $6 \times 10^4$  K, but the function is rather slowly varying with temperature over a reasonable temperature range for C IV. We see from (1) that if the absence

of a self-reversal implies  $\tau_0 \leq 1$ , we may derive a lower limit to  $P_e$  from the observations. In Table I we list these limits for  $P_e$ , and implied limits for  $N_e$  at a temperature of  $6 \times 10^4$  K. The absolute integrated line intensities for these events are taken at the maximum intensity for C IV, and they were obtained by the same method used by Lites, Hansen, and Shine (1979).

If we consider that the blueshift of event 2 represents an evaporation of chromospheric material into the flare coronal loops, we can obtain a lower limit to the total mass flux evaporated by knowing the flare area. Assume that the area of the flare that is participating in the evaporation in the transition zone is equal to that of the off-band  $H\alpha$  kernel from the flare patrol photographs:  $3.2 \times 10^{17}$  cm<sup>2</sup>. Using the lower limit to the density given in Table 2, and a velocity of  $10$  km s<sup>-1</sup> for a duration of 40 seconds, one obtains that at least  $1.5 \times 10^{13}$  grams are evaporated into the corona.

We now postulate that the increase in the soft x-ray emission of event 2 is due largely to the same evaporated chromospheric material. Datlowe, et al. (1974) deduced a similar physical picture for flare x-ray plasmas upon the time dependence of the temperature and emission measure of a large number of x-ray events. The onset of the rapid increase in the x-ray flux is seen in figure 2 to correspond to the occurrence of the blue-shifted profile. Given the emission measure for the coronal flare plasma, one may estimate the total coronal mass involved in the flare. The emission measure is defined as

$$E = N_e^2 V,$$

where  $N_e$  is the electron density and  $V$  is the emitting volume. The proton number density is approximately equal to the electron density, so

$$E \approx N_e M/m_p,$$

where  $M$  is the x-ray emitting coronal mass and  $m_p$  is the proton mass. If we assume pressure equilibrium between the transition-zone and corona in the flare plasma, we set a lower limit to  $N_e \geq 2.9 \times 10^9 \text{ cm}^{-3}$  at a temperature of  $15 \times 10^6 \text{ K}$ . This implies  $M \leq 4.0 \times 10^{14}$ . Note that this relationship resulted without any assumption about the flare volume. Typical flare densities in the corona are larger than our lower limit by as much as two orders of magnitude. A quite reasonable flare density of  $6 \times 10^{10}$  would cause the derived coronal mass to agree with the mass estimated to flow through the transition-zone. Similarly, transition-zone densities greater than our lower limit would force better agreement between the coronal and transition-zone masses.

## SUMMARY AND DISCUSSION

We have observed the chromospheric, transition-zone, and coronal response to the solar flare energy release for the entire time history of several small flares. We summarize the observational results in the following:

1) The impulsive brightening of the C IV transition-zone line is usually preceded by rapid downflow of material at measured velocities of  $80 \text{ km s}^{-1}$  or more.

2) This dynamic property of the transition-zone often precedes the soft x-ray impulsive brightening.

3) The time series of C IV profiles before, and continuing after in some events, frequently show evidence of rapid mass motions (usually redshifts).

4) The rapid brightening in the C IV line is accompanied by an attendant rapid brightening in the background intensity, implying significant energy input to the temperature minimum region during the impulsive phase of the flares.

5) Near the maximum brightening of C IV, we have observed a reversal from a downflow to an upflow of material in the most energetic C IV event observed. We interpret this as evidence for chromospheric evaporation, and the amount of material seen to evaporate is consistent with the added emission in the coronal loops as observed in soft x-rays.

6) The impulsive  $H\alpha$  chromospheric enhancement seems to start at the same time as the brightening in C IV, to within the time resolution of the observations for which we have coordinated data.

7) Soft x-ray emission always peaks well after the maximum of C IV, and the C IV impulsive brightening during the initial phases of the flares resembles the time derivative of the x-ray flare.

8) Impulsive microwave emission, when it accompanies an event, seems to start at the same time as the initial rise in the C IV emission.

The observational evidence presented here appears to indicate that the initial, impulsive release of flare energy directly causes, or is the result of, rapid and short-lived downflows in the transition-zone. If the microwave bursts are caused by gyro-synchrotron radiation from particle beams (and the bursts that occur do have significant circular polarization), then in at least one event (event 2) particle beams do not seem to be involved. We suspect that the particle streams are the result of the flare energy release, and are not the cause of the heating in the transition zone and lower. The time behavior of the soft x-ray emission seems to be a result of the filling of the coronal loops with evaporated material as a result of rapid heating of the chromosphere to transition-zone and coronal temperatures.

**ACKNOWLEDGEMENTS**

We greatly appreciate the receipt of microwave data from Dr. S. Enome at the Tokokawa Observatory. We also thank Capt. M. R. Fourroux of the U.S. Air Force for providing a time sequence of H $\alpha$  photographs for the 6 April 1978 event, and the U.S. Air Force for providing H $\alpha$  flare patrol photographs of the March 30, 1976 event from their Ramey, Puerto Rico station. We acknowledge D. W. Datlowe and R. C. Canfield for useful discussions. This research was supported by the National Aeronautics and Space Administration grants NAS 5-11363, NAS 5-22411, and by the Lockheed Independent Research Program.

## Figure Captions

Figures 1 - 4. The time dependence of the flare brightening in C IV (top curves), soft x-rays, and microwave flux at 3750 MHz (where applicable) is given for the 1976 March 30, and 1978 April 6, April 11, and April 15 events respectively. Also shown are the time developments of the x-ray flare emission measure (dashed curves) and temperature as derived from best fits of theoretical spectra of an isothermal plasma to the x-ray spectra. Uncertainty estimates expected due to photon counting statistics are given near the minimum and maximum intensity and flux of C IV and x-rays in figure 1. In figures 2-4, the uncertainties near maximum of the flare are too small to plot, but they scale as the square-root of the respective intensity or flux. We have no estimation of the uncertainty in the microwave data, and uncertainties of the x-ray temperature and emission measure depend on the validity of the model assumed for the flare plasma.

Figure 5. The time series of C IV line profiles (5a) is given for event 2. The profile in 5b is the preflare average of the first six profiles shown, and the dashed vertical lines in 5b, 5c, and 5d give the line-center position of the preflare average. The profiles in figures 5c (profile 13) shows a redshifted component of  $65 \text{ km s}^{-1}$ , and the profile in 5d (profile 14) is blueshifted by about  $10 \text{ km s}^{-1}$  relative to the preflare average. The intensity scales are uncalibrated, and are given in photon counts per 4-second gate time.

Figure 6. H $\alpha$  flare-patrol sequence for event 1. The slit of the OSO-8 CU instrument was located over the brightening seen just inside the sunspot. All photographs are taken on-band, except for these labeled 21.40 UT Blue and 21.41 UT Red, which were taken with the filter shifted  $0.5 \text{ \AA}$  to the blue and red, respectively.

Figure 7. H $\alpha$  flare patrol photograph of event 2 taken at  $23^{\text{h}} 26^{\text{m}} 21^{\text{s}}$  on 1978 April 6. The long dimension (20 arcseconds) of the CU OSO-8 slit lay between the tips of the arrows. The other dimensions of the slit had an effective width of about 2 arcseconds. The flare was a compact and short-lived event in H $\alpha$ .

Figure 8. The differential of the x-ray flux (solid curve) is plotted along with the C IV intensity (linear scale-dashed curve) as a function of time for events 2, 3, and 4. The normalization of both quantities is arbitrary, and the time scale is given in minutes from C IV maximum intensity.

## References

- Athay, R. G. and White, O. R. 1980, Ap. J. (to appear in March).
- Brueckner, G. E., Patterson, N. P., and Scherrer, V. F. 1976, Solar Phys. 47, 127.
- Bruner, E. C. 1977, Space Sci. Instr., 3, 369.
- Bruner, E. C. and Lites, B. W. 1979, Ap. J. 228, 322.
- Canfield, R. C., Cheng, C.-C., Dere, K. P., Dulk, G. A., McLean, D. J., Robinson, R. D. Jr., Schmahl, E. J., and Schoolman, S. A. 1980, Appendix A of Solar Flares, A Monograph from Skylab Workshop II. (High Altitude Observatory, Boulder, Colorado).
- Chipman, E. G. 1978, Ap. J. 224, 671.
- Cook, J. W., and Brueckner, G. E. 1979, Ap. J. 225, 650.
- Datlowe, D. W., Hudson, H. S., and Peterson, L. E. 1974, Solar Phys. 35, 193.
- Foukal, D. V., Huber, M. C. E., Noyes, R. W., Reeves, E. M., Schmahl, E. J., Timothy, J. G., Vernazza, J. E., and Withbroe, G. L. 1974, Ap. J., 193, L143.

Lites, B. W. 1980, Solar Phys. (in press).

Lites, B. W., Hansen, E. R. and Shine. R. A. 1980, Ap. J. (in press).

Machado, M. E., Emslie, A. G., and Brown, J. C. 1978, Solar Phys. 58, 363.

Svestka, Z. 1976, Solar Flares (Dordrecht:Reidel).

Tucker, W. H. and Koren, M. 1971, Astrophys. J. 118, 283.

Wolfson, C. J., Acton, L. W., and Gilbreth, C. W. 1975, Mapping X-Ray Heliometer of OSO-8, Final Report, NAS-CR-144710.

Wolfson, C. J., Acton, L. W., Leibacher, J. W., and Roethig, D. T. 1977, Solar Phys. 55, 181.

Event	1	2	3	4
Date	30 March 1976	6 April 1978	11 April 1978	15 April 1978
Start Time, UT(C IV)	2139	2317	0409	0811
McMath Plage Region	14179	15221	15221	15235
Disk Position $\mu$	0.7	0.9	0.5	0.9
<u>H<math>\alpha</math> Flare</u>				
H $\alpha$ Flare Type (Source)	Subflare (USAF-Ramy, P.R.)	Subflare (USAF-Soon Network, White Sands, N.M.)	1W ( <sup>1</sup> )	Bright Subflare ( <sup>1</sup> )
Area (cm <sup>2</sup> )	$7.6 \times 10^{17}$	$3.2 \times 10^{17}$ ( <sup>2</sup> )	$5.5 \times 10^{18}$ ( <sup>1</sup> )	$1.6 \times 10^{18}$ ( <sup>1</sup> )
<u>C IV Flare</u>				
Fraction of OSO-8 Slit Covered by Flare( <sup>3</sup> )	0.45	0.48	1.0	1.0
I/I <sub>0</sub> (C IV)	5.4	40.1	14.6	71.
I/I <sub>0</sub> (Background)	1.0	16.	5.2	10.9
Maximum <sub>1</sub> Redshift (km s <sup>-1</sup> )	45	90	60	>20
Total Line Broadening Velocity <sub>4</sub> (Km s <sup>-1</sup> )	35	37	25	50
Risetime at C IV Event ( $\zeta$ )	100	300	90	80
Integrated Intensity <sub>4</sub> (Erg cm <sup>-2</sup> s <sup>-1</sup> Ster <sup>-1</sup> )	$2.8 \times 10^3$	$5.4 \times 10^5$	$5.9 \times 10^4$	$5.4 \times 10^5$

Maximum Intensity <sup>2</sup> (Erg cm <sup>-2</sup> s <sup>-1</sup> Ster <sup>-1</sup> Hz <sup>-1</sup> )	8.5 x 10 <sup>-9</sup>	8.1 x 10 <sup>-7</sup>	1.3 x 10 <sup>-7</sup>	5.3 x 10 <sup>-7</sup>
Electron Pressure (dynes cm <sup>-3</sup> )	≥ 0.04	≥ 6.0	≥ 0.47	≥ 2.1
Electron Densities (cm <sup>-3</sup> )	≥ 5 x 10 <sup>9</sup>	≥ 7 x 10 <sup>11</sup>	≥ 5.6 x 10 <sup>10</sup>	≥ 2.5 x 10 <sup>11</sup>
<u>X-Ray Flare</u>				
Maximum Intensity (1-8 Å) <sup>1</sup> (Erg s <sup>-1</sup> )	1.2 x 10 <sup>24</sup>	8.7 x 10 <sup>24</sup>	2.3 x 10 <sup>25</sup>	7 x 10 <sup>25</sup>
I <sub>max</sub> / I <sub>preflare</sub>	3.2	4.1	8.4	88
Maximum Temperature (10 <sup>6</sup> K)	12	15	18	19
Maximum Emission Measure (cm <sup>-3</sup> )	5 x 10 <sup>47</sup>	7 x 10 <sup>47</sup>	2.4 x 10 <sup>48</sup>	1.0 x 10 <sup>49</sup>

<sup>1</sup>From SOLAR GEOPHYSICAL DATA

<sup>2</sup>Off-band H $\alpha$  Kernel Size

<sup>3</sup>Derived from H $\alpha$  Images and Spacecraft Pointing Data

<sup>4</sup>Taken at Maximum Intensity

FIG. 1

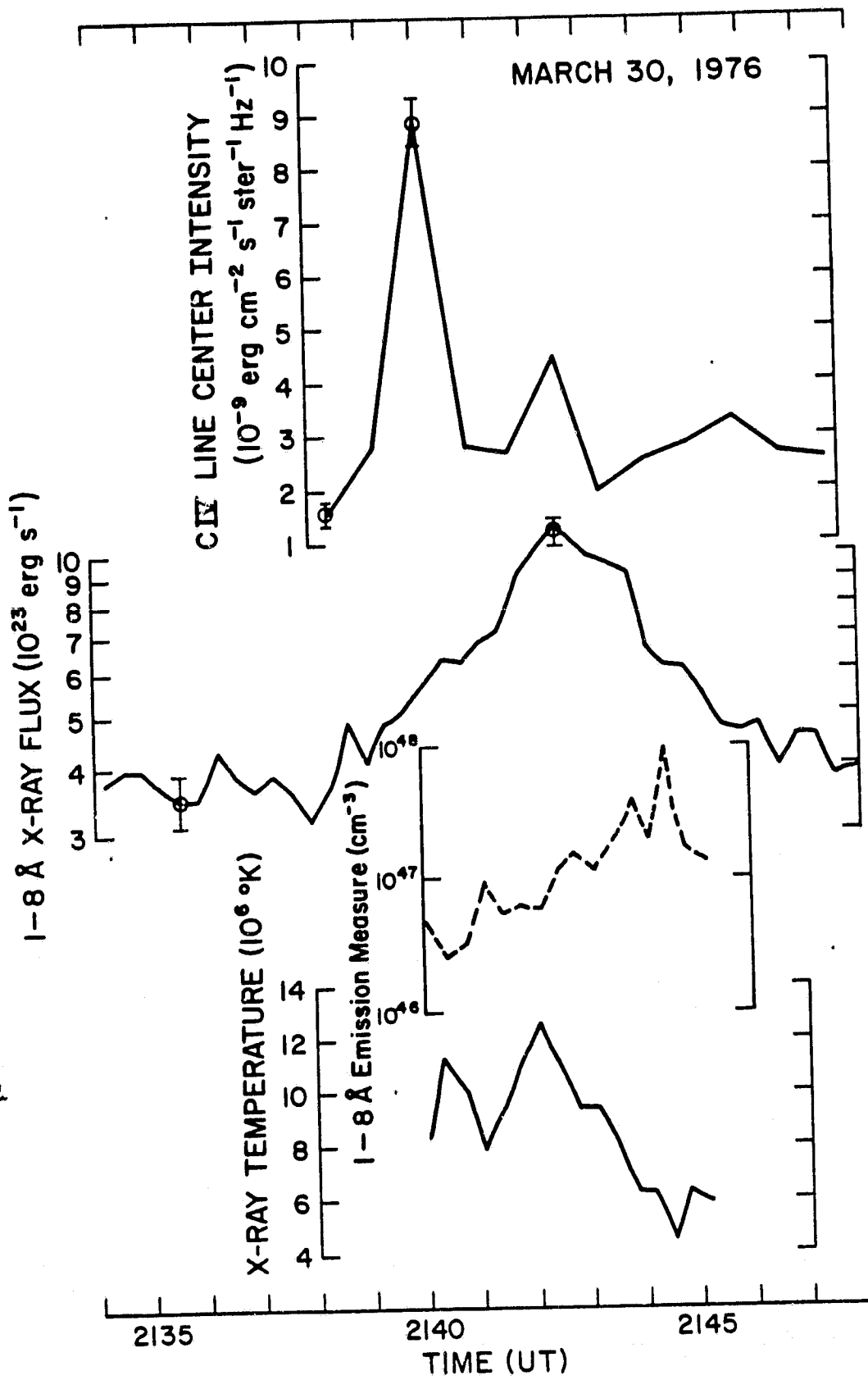


FIG 2

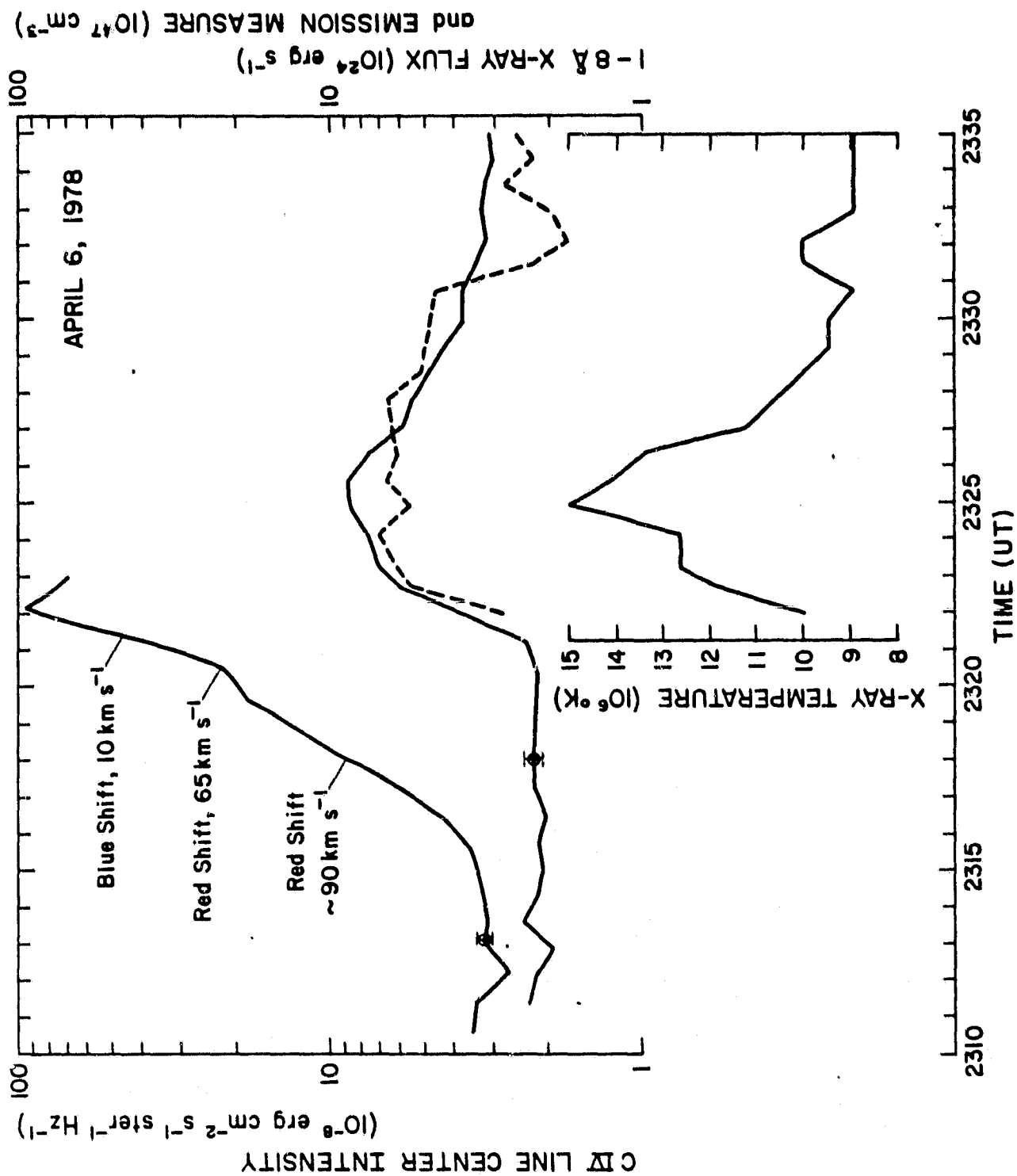


FIG 3

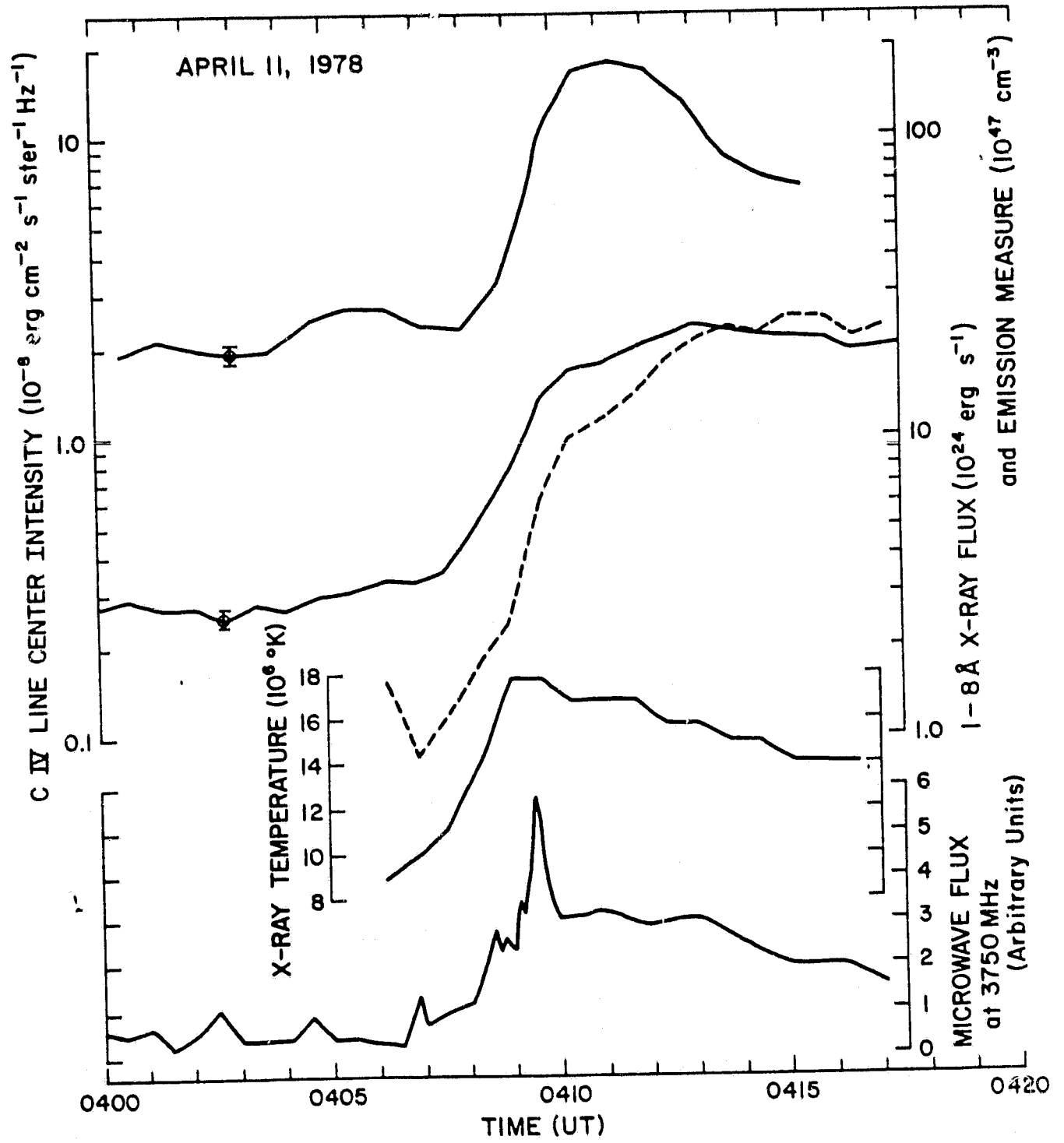
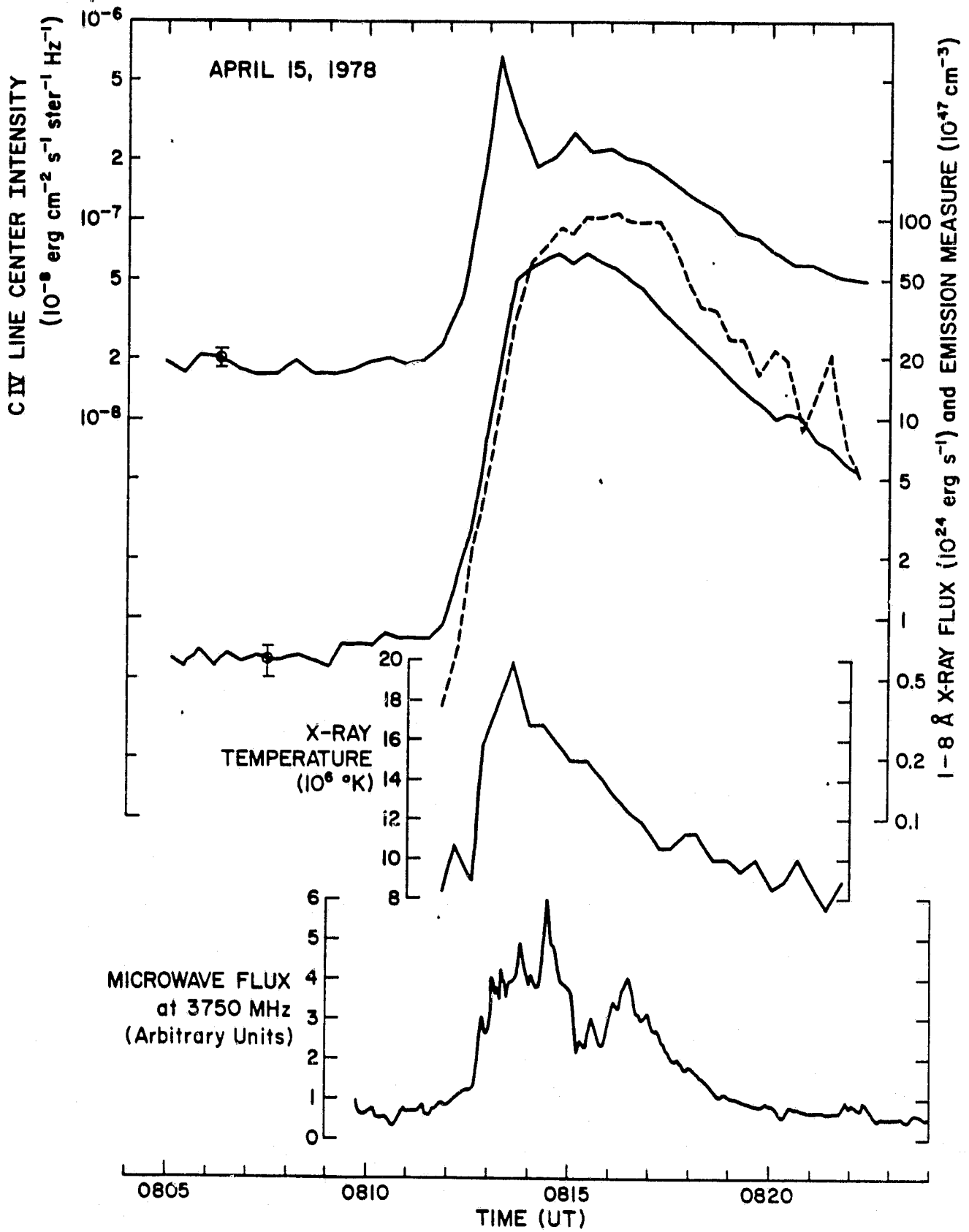
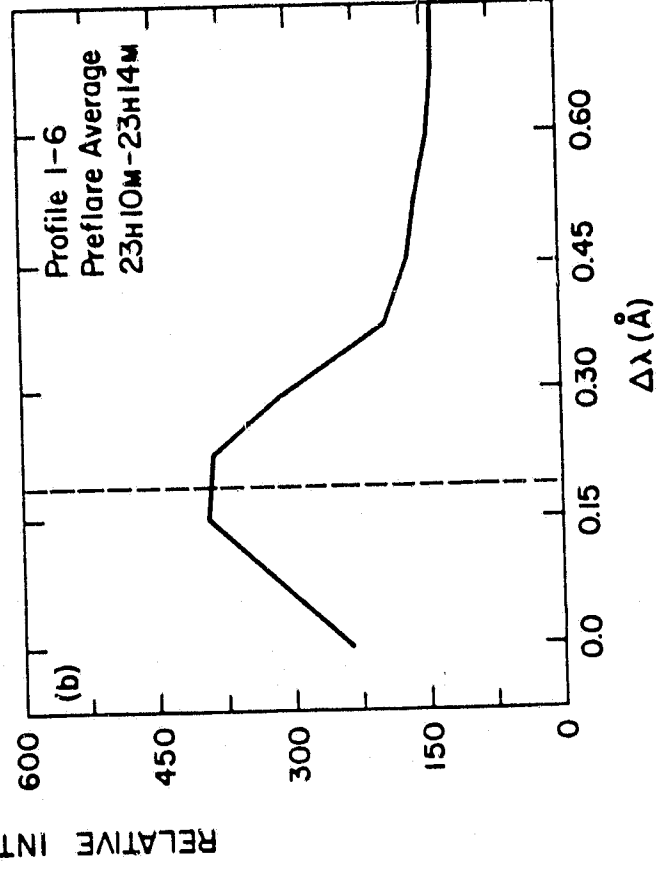
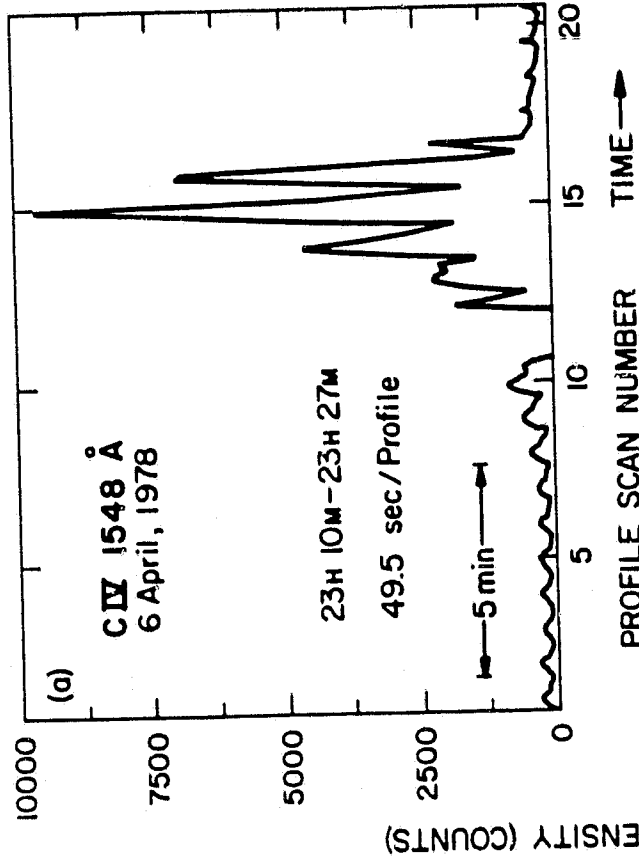
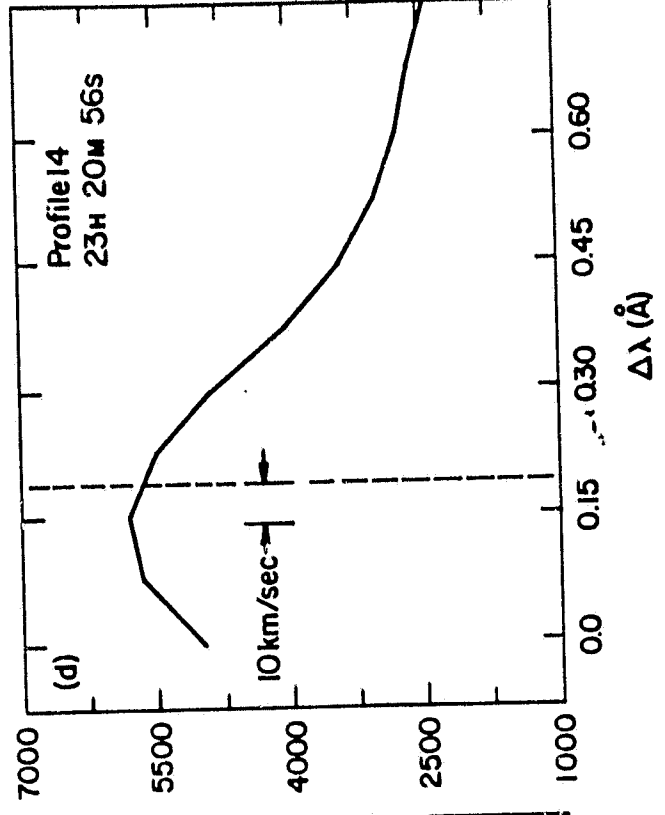
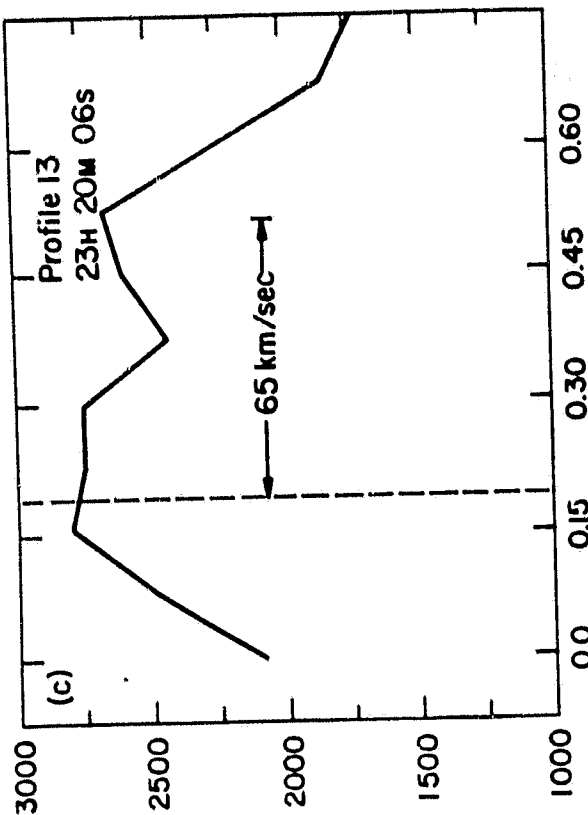


FIG. 4





RELATIVE INTENSITY (COUNTS)

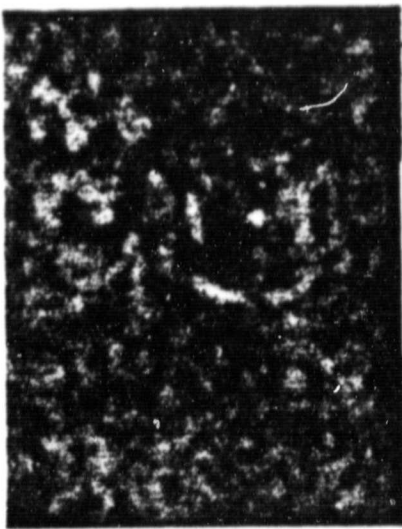
FIG. 6

N ↑

H- $\alpha$  RAMEY, PUERTO RICO  
MARCH 30, 1976



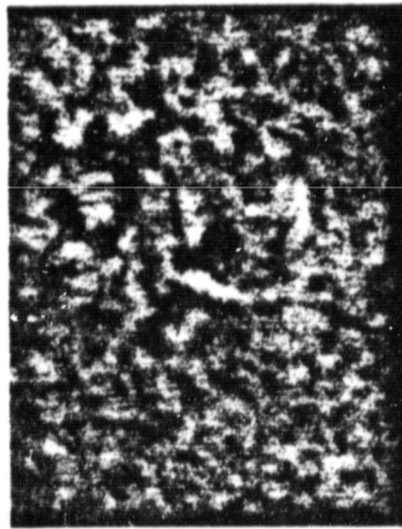
21:42 UT



21:41 UT RED



21:40 UT



21:40 UT BLUE



21:39 UT



21:49 UT

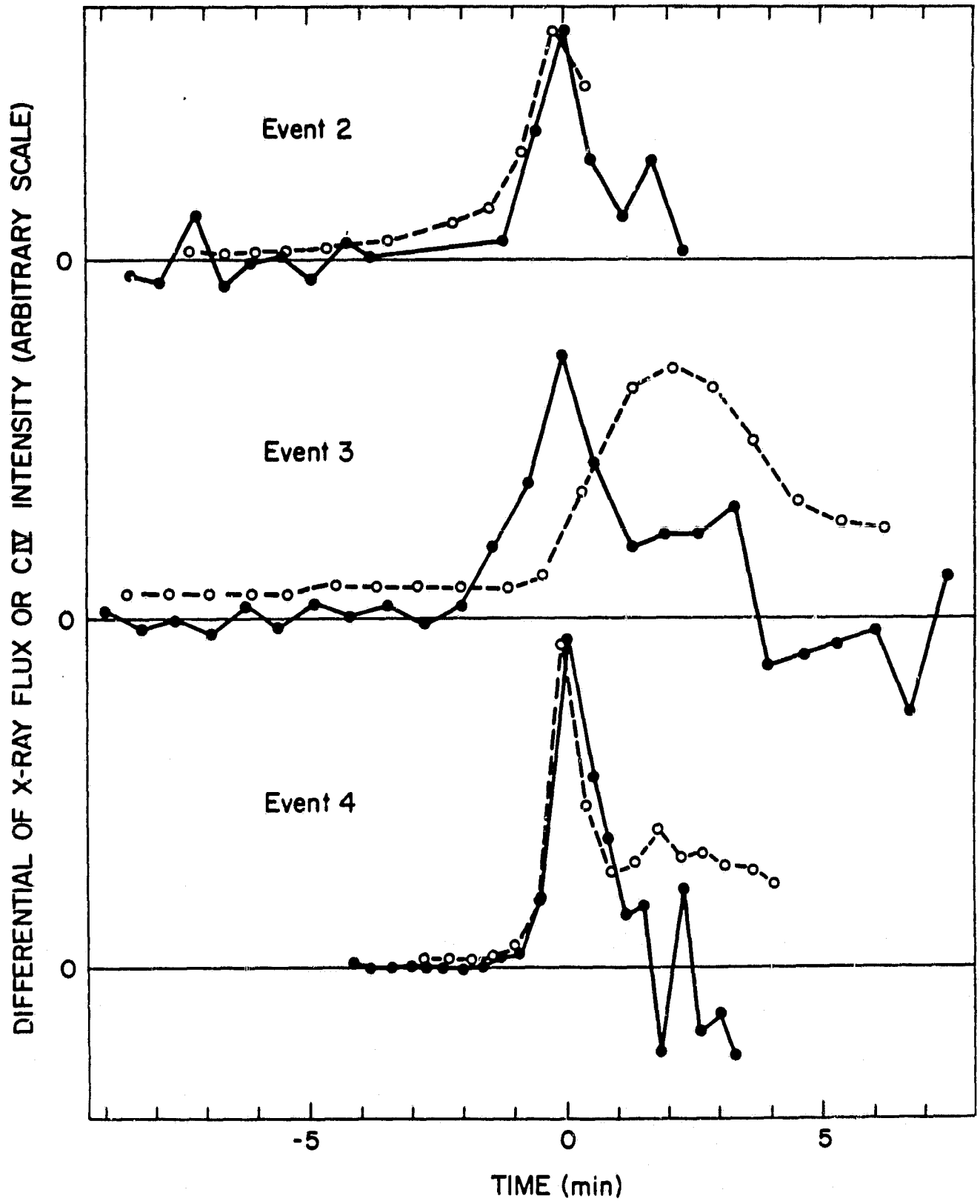
ORIGINAL PAGE IS  
OF POOR QUALITY

FIG. 7



ORIGINAL PAGE IS  
OF POOR QUALITY

FIG. 8



OSO-8 OBSERVATIONAL LIMITS TO THE ACOUSTIC  
CORONAL HEATING MECHANISM

E.C. Bruner, Jr.

Accepted for publication in The Astrophysical Journal

OSO-8 Observational Limits to  
the Acoustic Coronal Heating Mechanism

E.C. Bruner, Jr.  
Lockheed Palo Alto Research Laboratory  
Received 1979 October 22

ABSTRACT

An improved analysis of time resolved line profiles of the C IV resonance line at  $1548\text{\AA}$  has been used to test the acoustic wave hypothesis of Solar Coronal Heating. It is shown that the observed motions and brightness fluctuations are consistent with the existence of acoustic waves. Specific account is taken of the effect of photon statistics on the observed velocities and a test is devised to determine whether the motions represent propagating or evanescent waves. It is found that on the average, about as much energy is carried upward as downward such that the net acoustic flux density is statistically consistent with zero. The statistical uncertainty in this null result is three orders of magnitude lower than the flux level needed to heat the corona.

Subject Headings: line profiles - Sun: corona - Sun: spectra

## Introduction

In an earlier study (Bruner, 1978), OSO-8 observations of the transition zone line of C IV at 1548 Å were used as a diagnostic with which to search for evidence of wave motion in the solar atmosphere. The study showed that while such evidence could occasionally be found, the observed rms particle velocities implied an upper limit to the flux of acoustic waves that was inadequate to account for coronal heating. An independent study by R.G. Athay and O.R. White (1978), based on measurements of the Si II line width and model atmosphere calculations reached a similar conclusion. A third investigation by Bruner and McWhirter (1979) used measurements of the average width and symmetry properties of the  $\lambda 1548\text{\AA}$  carbon IV line together with various theoretical arguments to set upper limits on the flux of acoustic and Alfvén waves. It also failed to support the acoustic heating hypothesis. Athay and White (1979) have computed average power spectra of the fluctuations in the C IV line intensity and position using a more extensive data set than the one analyzed by Bruner (1978). They were able to establish the existence of statistically significant wave motions in about 20% of the observations, but again found the flux to be inadequate for coronal heating.

The purpose of this paper is to place still more stringent upper limits on the acoustic energy flux by taking specific account of two effects. These are 1) the contribution of photon statistics to the observed rms velocity signal and 2) the possibility that an observed wave may contain both propagating and evanescent components.

## The Effect of Photon Statistics

Consider the noise problem first. OSO-8 velocity studies consist of sets of repeated line profile measurements carried out at a fixed pointing position on the solar disk. The spectrometer accepted an angular field of  $1 \times 20$  arc seconds. Since the OSO-8 spectrometer is a single channel instrument (Bruner, 1977), the wavelength drive must be scanned across the line once for each profile measurement. In the case of the Carbon IV experiments, each scan sampled eleven wavelengths spaced at 0.075 Å intervals. Integration times at each wavelength were either 4 or 2 seconds and the times required to scan the profile once were 49 and 27 seconds, respectively. Observing periods were limited by orbital mechanics to a maximum of one hour, permitting about 70

profile measurements to be made in the 49 second mode and about 130 in the 27 second mode. In the material to follow, I will refer to the 49 second observations as data set 1 and the 27 second observations as data set 2.

Analysis of the data was based upon the computation of the zeroth moment

$$M_0(i) = \frac{1}{n} \sum_{i=1}^n N_{ij}, \quad 1)$$

which was proportional to the integrated line intensity, and the first moment

$$M_1(j) = \frac{\sum_{i=1}^n i N_{ij}}{\sum_{i=1}^n N_{ij}}, \quad 2)$$

which gives a measure of the line position relative to the start of the scan. In this notation,  $N_{ij}$  is the observed photon count at the  $i$ th wavelength in the  $j$ th measurement of the profile. The value of  $n$  is 11.

In the absence of both photon noise and fluctuations in the source, the profile would be constant; that is, for a given  $i$ , the values of  $N_{ij}$  would be the same for all  $j$  and the variances of  $M_0$  and  $M_1$  would be zero. Since photon counting is a statistical process, there will be fluctuations in the measured  $N_{ij}$ 's of the order of  $\sqrt{N_{ij}}$  even in the case of a constant source. Since the  $N_{ij}$ 's appear with different weights in the numerator and denominator of the defining expressions for the moment, statistical fluctuations in the  $N_{ij}$ 's will produce non zero variances in the moments.

I have used a monte-carlo technique to evaluate the photon noise contribution to the rms velocity signal for the intensity levels and line widths appropriate to the Carbon IV studies. Artificial Gaussian profiles of the form

$$N_{ij} = B + A \text{ EXP } [-(6-i)^2/w^2] \quad 3)$$

$i=1, 11$   
 $j=1, 64$

were generated, where A represented the amplitude, B the stray light background in the spectrometer and w was adjusted to give a full width at half intensity of about 2.5 sampling intervals. Each profile was centered on the 6th wavelength point. The profiles were then perturbed at each wavelength with random numbers whose expectation values were the square roots of the respective intensities. The profiles were analyzed in blocks of 64 with the aid of the moment representations defined above.

The computations were carried out on a Commodore 2001 computer using the system supplied random number generator. The generator was seeded with the instantaneous value of the system clock in order to improve the uniformity of the random number distribution. The uniformly distributed numbers were converted to a gaussian distribution via the Box-Muller transform (Dahlquist and Bjork, 1974). The background level was taken to be 40 counts for the 49 sec data and 20 counts for the 27 sec data. Amplitudes ranged from ten to several thousand. The whole series of computations was run several times in order to evaluate the uncertainties in the size of the photon noise contribution.

The results of the numerical simulation are shown in Figure 1. As one would expect, the fainter profiles show a larger spurious velocity signal than the brightest ones. The rms value of the noise produced velocity signal ranges from about 400 m/sec for the brightest profiles observed by OSO-8 to about 5 km/sec for the faintest. The noise velocity is well represented by the expression

$$\log \sigma(u) = A_0 + A_1 \log(\bar{M}_0) + A_2 (\log(\bar{M}_0))^2 + A_3 (\log(\bar{M}_0))^3 \quad 4)$$

where  $\sigma(u)$  is the standard deviation of the line position expressed as a velocity and

$$\bar{M}_0 = \frac{1}{K} \sum_{i=1}^K M_0(i) \quad 5)$$

is the total number of photons counted per channel in the average line profile. The value of K is 64. The expression was derived by fitting a third degree polynomial to the data of Figure 1 using the method of least squares. The intensity uncertainties derived from the simulation vary as the square root of the total photon count in the average line profile, again as one would expect.

In Figure 2, the noise predictions are compared with the earlier analysis of data set 1 (Bruner, 1978). Although observed velocities exceed the predicted noise contributions at all intensity levels, much of the velocity signal at the low intensity end of the distribution is seen to be due to photon noise, as suggested in the earlier work. In the case of the intensities, however, the variances in the observed intensities are larger than those predicted from photon statistics at all intensity levels. This is in agreement with the results of Athay and White (1979) and implies that the fluctuations are inherent in the sun itself. Such fluctuations are, indeed, expected if acoustic waves are present.

#### Noise Corrections

In order to correct the observed velocities for the effect of noise, I have assumed that the intrinsic line position fluctuations and those due to photon noise are statistically independent and combine in quadrature. That is,

$$\sigma_{\text{obs}} = (\sigma_n^2 + \sigma_i^2)^{1/2} \quad 6)$$

where  $\sigma_{\text{obs}}$  is the observed standard deviation in line position  $\sigma_n$  the standard deviation expected from photon noise, and  $\sigma_i$  that due to solar atmospheric motions. This may be rearranged as

$$\sigma_i = (\sigma_{\text{obs}}^2 - \sigma_n^2)^{1/2} \quad 7)$$

where the values  $\sigma_n$  are to be determined from the empirical expression derived from the monte-carlo simulation. In those cases where  $\sigma_n > \sigma_{obs}$ , the value of  $\sigma_1$  is take to be zero.

The results for data set 1 are shown in Figure 3. It is seen that the systematic trend of increasing velocities at low intensities has been largely eliminated, although the observations showing the largest rms velocities were found in the quiet network (where intensities are small). The average velocity for the 28 quiet sun observations of data set 1 was  $2.3 \pm 0.3$  km/sec. The average for all 44 observations in data set 1 was  $2.2 \pm 0.2$  km/sec. The uncertainties quoted in each case are the standard deviations in the mean computed from the corrected data; no estimate of systematic error has been included.

Similar results were obtained for data set 2. The rms velocities, before and after noise correction are plotted in Figures 4 and 5 as functions of the corresponding observed intensities. Here again, we see that the systematic dependence of the observed velocity on intensity is primarily due to the effect of photon counting statistics. The corrected rms velocity for the mean of all 164 observations of data set 2 was  $0.65$  km/sec  $\pm$   $0.59$  km/sec. This value is probably too low as a result of overcorrection for photon noise. Many of the observations were made later in the mission when the sensitivity and hence the background contribution to the noise were lower. An independent calculation in which the correction was knowingly underestimated gave a result of  $1.6 \pm 0.7$  km/sec for this data set. This value may be taken as an upper limit to the rms velocity determined from this data set.

#### Consistency Test for Waves

We turn now to the question of whether observed fluctuations in the line position and intensity correspond to acoustic waves and, if so, whether the waves are propagating energy. The presentation will be in two parts. In the first, I will show that the orbital averages of the observed intensity and velocity modulations are consistent with the presence of acoustic waves. In the second, I will use the cross correlation computed between intensity and velocity to estimate the average acoustic power density transmitted by the waves. This calculation corrects for the effects of non-propagating (standing or evanescent) wave modes.

The question of character of the waves was considered by Noyes and Leighton (1963) in their analysis of oscillations in the photosphere and low chromosphere. Their treatment compared the measured cross correlation between intensity and velocity fluctuations to the phase shifts predicted by the acoustic-gravity wave equation under the assumption that the intensity fluctuations were primarily caused by temperature modulation of the atmosphere by the waves. In computing the temperature fluctuations, they considered heating by conduction from hot granules, by adiabatic compression of the waves, and cooling by radiative losses. The presence of multiple heating terms had the effect of introducing a phase shift between the velocity and intensity modulations. This work was successful in predicting the main features of the observed dependence of phase on the height of formation of the line. The predicted phase shift for a propagating wave approached zero at the top of the chromosphere.

In considering the ultraviolet transition zone lines, the situation is somewhat different. The most important factor controlling the intensity fluctuations is the electron density, rather than the electron temperature (Lites and Hansen, 1978). The relevant lines are optically thin and densities are sufficiently low that only collisional excitation and radiative de-excitation need be considered. The collisional excitation rate is

$$C_{12} = \alpha A N_e^2 \frac{8k}{m_e} \sigma_\tau \pi a_0^2 \frac{T^*}{\sqrt{T}} \exp\left(-\frac{T^*}{T}\right) \quad 8)$$

where  $T^* = hv/k$  is the excitation temperature.  $A$  is the abundance of Silicon relative to Hydrogen,  $\alpha$  is the fraction of Silicon IV relative to all stages of ionization,  $N_e$  is the electron density,  $k$  is Boltzmann's constant, and  $m_e$  is the mass of the electron.  $\sigma_\tau$  is the ionization cross section at threshold and  $\pi a_0^2$  is the area of the first Bohr orbit.

In the presence of acoustic waves, the collisional excitation rate is modulated, due to the instantaneous changes in pressure and temperature. In the case of low amplitude adiabatic waves, the pressure modulation may be shown to be

$$\frac{\Delta P}{P} = \gamma \frac{u}{c} \quad 9)$$

where  $P$  is the pressure,  $\gamma$  is the adiabatic constant,  $u$  is the disturbance velocity of the wave and

$$c = \left( \frac{P\gamma}{\rho} \right)^{1/2} \quad 10)$$

is the sound velocity (Lamb, 1945). The pressure modulations will produce fluctuations in the electron density and temperature of

$$\frac{\delta N_e}{N_e} = \frac{u}{c} \quad 11)$$

and

$$\frac{\delta T}{T} = (\gamma - 1) \frac{u}{c} \quad 12)$$

respectively. The result of these perturbations on the collisional excitation rates will be to produce a modulation in the collision rate of\*\*\*\*\*

$$\frac{\delta C_{12}}{C_{12}} = 2 \frac{u}{c} + \left( \frac{T^*}{T} - 1/2 \right) (\gamma - 1) \frac{u}{c} \quad 13)$$

where the first term is the result of the density fluctuations and the second is due to temperature changes. For the Carbon IV lines at 1548 and 1550A, the values of  $T$  and  $T^*$  are both about 100,000°K so that their ratio is near unity. For these lines, assuming adiabatic waves, the contribution of the density term to the modulation exceeds that of the temperature term by a factor of 6. This is in sharp contrast with the situation in the visible, where the temperature fluctuations are the dominant effect (Noyes and Leighton, 1963).

In defining Equation 13, I have assumed that the ionization balance of carbon does not change as a result of the wave perturbations. This was done for two reasons. First, the temperature fluctuations are expected to be small

- only about 3% for waves with a velocity amplitude of 2 km/sec (based on the adiabatic case calculations prepared for Bruner and Lites, 1979) - so that a major restructuring of the atmosphere is not expected. If the process is not adiabatic, the temperature fluctuations are likely to be even smaller. The second point is that if the ionization balance does change dynamically, then the intensity modulation for a given wave amplitude will be greater. Thus, neglect of the effect will overestimate the pressure amplitude and hence the reported acoustic flux. Since we are interested in finding an upper limit to the flux, this is not troublesome.

The linear approximation is fairly good when the intensity modulation is below about 0.1, but breaks down at higher levels due to the formation of shocks. Bruner and Lites (1979) used the Rankin-Hugoniot relations to predict the intensity modulation produced by shocks giving rise to a range of disturbance velocities. Their curve is reproduced in Figure 6 together with the results of the linear calculation and the observations of data set 1.

The trend of the observations is in fairly good agreement with the predicted relation for sound waves, but it is seen that most of the observed velocities fall below the curve. This is to be expected, since in general the waves will be propagating at some angle to the line of sight. If on the average, the waves are observed at a 45 degree angle with respect to the line of sight, the expected velocities would be lower by a factor of the square root of 2. If the predicted curve is adjusted downward by this factor, it is seen to fall right in the middle of the observed distribution. It is clear that the observations are consistent with the existence of acoustic waves, at least as far as the orbital averages are concerned.

#### The Cross Correlation Test for Propagation

We turn now to the question of the energy transported by the waves. The instantaneous value of the acoustic flux density is the product of the overpressure and the disturbance velocity. The average power density will be the expectation value of this product computed over a suitable time interval (either an integral number of periods, or a time large compared to the longest period present)

$$\psi = \langle u\delta P \rangle = \frac{1}{\tau} \int_0^{\tau} u(t) \delta P(t) dt. \quad (14)$$

If  $u$  and  $\delta P$  are in phase, then the expectation value will be finite. If they are  $90^\circ$  out of phase, as in an evanescent or standing wave, then the expectation value will vanish. If  $u$  and  $\delta P$  are measured independently (as they are in the OSO-8 data), then this flux calculation is rigorous regardless of whether or not the waves are propagating or whether they are periodic. Moreover, the sign of the expectation value will tell whether the energy is propagating toward or away from the observer.

An equivalent expression for the flux is

$$\psi = P_o u_{\text{rms}} \left( \frac{\delta P}{P_o} \right)_{\text{rms}} \frac{\langle u \delta P \rangle}{(\langle u^2 \rangle \langle \delta P^2 \rangle)^{1/2}} \quad (15)$$

where the quantity in square brackets is the cross correlation function of  $u$  and  $\delta P$  computed for zero lag. In terms of the observed intensity, the expression becomes

$$\psi = P_o \gamma \left[ 2 + \left( \frac{T^*}{T} - \frac{1}{2} \right) (\gamma - 1) \right]^{-1} u_{\text{rms}} \left( \frac{\delta I}{I} \right)_{\text{rms}} \frac{\langle u \delta I \rangle}{(\langle u^2 \rangle \langle \delta I^2 \rangle)^{1/2}}$$

provided that the waves are either adiabatic ( $\gamma = 5/3$ ) or completely isothermal ( $\gamma = 1$ ). For intermediate cases, a phase shift will be introduced between the density and temperature fluctuations with the result that the intensity and pressure fluctuations will be out of phase. Under these conditions, the cross correlation would need to be calculated for a lag other than zero. The effect is not a serious one for the ultraviolet lines, since the density effect dominates. The worst case phase error of  $\tan^{-1} 1/6$  would occur if the pressure and temperature variations were in quadrature. Ignoring the phase shift would result in a cosine error of less than 2% in the cross correlation.

In computing the flux densities from data set 1, I assumed pressures of  $0.2 \text{ dyne cm}^{-2}$  for the quiet regions and  $2 \text{ dyne cm}^{-2}$  for active regions (Withbroe and Noyes, 1977). The rms velocities and intensity modulations were computed after first subtracting a third degree polynomial to correct for the effects of orbital motion and changing temperature gradients (Bruner, 1978).

The cross correlations were computed from the cross power spectra, using a fast Fourier transform algorithm (Bracewell, 1965). I arbitrarily chose the adiabatic case, which leads to fluxes about 40% larger than for isothermal waves.

The results of the analysis of data set 1 are summarized in Figure 7 and Table 1. Each entry represents one orbit of observations lasting about 1 hour and is identified by the file name under which the data are stored in the OSO-8 archives (Hansen and Bruner, 1979). Absolute intensities were assigned based on a calibration rocket experiment conducted by G.J. Rottman (1976). The rms velocities have been corrected for photon noise as discussed in the first part of this paper. The intensity modulations, however, have not and as a consequence, are too large by an average of about 10%.

The sign convention in both the cross correlation and the acoustic flux density is such that positive values indicate that increased brightness correlates with red shifts, corresponding to wave propagation away from the observer. Both positive and negative values are found with about equal frequency. The magnitudes of the cross correlations vary from less than 1% to 72%, with the overall average being about 16%. The flux densities in the quiet region observations range from zero (observed rms velocity less than predicted noise contribution) to  $6.2 \times 10^3 \text{ erg cm}^{-2} \text{ sec}^{-1}$ . A number of examples of evanescent wave motions are seen in which the rms velocity is substantial, but the cross correlation is low. The average net flux for all 28 quiet region observations (taking account of the sign) is  $+0.54 \times 10^3 \pm 0.32 \times 10^3 \text{ erg cm}^{-2} \text{ sec}^{-1}$ . The corresponding average for the 16 active region observations was  $-1.8 \times 10^3 \pm 6.8 \times 10^3 \text{ erg cm}^{-2} \text{ sec}^{-1}$ . The reported uncertainties are the standard deviation in the mean. The net acoustic flux density in the quiet region is, at best, marginally significant while that for the active regions is statistically indistinguishable from zero.

In computing the flux for data set 2, I took the pressure to be proportional to the average intensity of the C IV line following the work of Haisch and Linsky (1976). Pressures ranged from about  $0.2 \text{ dynes cm}^{-2}$  to about  $4 \text{ dynes cm}^{-2}$ . Again, the cross correlation function showed downward propagation about as frequently as upward, with magnitudes of the correlation ranging from 0 to about 0.65. The results are plotted in Figure 3. The net flux, average

over all 164 observations, was  $0.14 \times 10^3 \pm 0.28 \times 10^3 \text{ erg cm}^{-2} \text{ sec}^{-1}$  directed downward. Here again, the uncertainty in the mean exceeds the net flux, so that the latter is statistically consistent with zero.

### Discussion

The energy requirement to maintain the Solar Corona against energy losses due to radiation, conduction, and the solar wind has been estimated to be in the range  $2 - 6 \times 10^5 \text{ erg cm}^{-2} \text{ sec}^{-1}$  (see, for example, Athay, 1976). In the earlier analysis of data set 1 (Bruner, 1978) an upper limit on the acoustic energy flux passing the transition zone was found to be  $7 \times 10^4 \text{ erg cm}^{-2} \text{ sec}^{-1}$ , which is too low by about a decade to heat the corona. This upper limit was based on a 3 km/sec velocity amplitude, the assumption that it represented upward propagating waves, and the assumption of 8 independently moving emission elements in the 1" x 20" field of view. Athay and White (1979) used a 3 km/sec rms velocity with somewhat different assumptions to derive an upper limit of  $2 \times 10^3 \text{ erg cm}^{-2} \text{ sec}^{-1}$ . The noise corrections of the present paper show that the rms velocity should be revised downward to at most 2.2 km/sec (less for data set 2), which reduces both estimates of the upper limit by about a factor of 2.

Much more significant, is the observation that acoustic waves appear to propagate downward about as frequently as upward at transition zone heights so that the net observed flux is effectively zero. The statistical uncertainty in the mean of  $300 \text{ erg cm}^{-2} \text{ sec}^{-1}$  gives the largest upward acoustic flux that could be admitted by these data and is three orders of magnitude too low to explain coronal heating. This observation appears to be catastrophic to the acoustic wave hypothesis.

I should point out that in the presence of noise we may expect the cross correlation function to be reduced, resulting in an underestimate of the energy flux. A detailed evaluation of the factor by which the sensitivity is reduced has not been made. However, it should be no smaller than 0.3 which is the peak absolute value of the cross correlation curve averaged over all orbits. If the cross correlation was seriously reduced by noise, then one would expect low values of the reported flux to be preferentially associated with low intensities. Inspection of Table I and Figures 7 and 8 show that this is not the case; rather, both low and relatively high levels of acoustic flux density can be found at all intensity levels.

## Conclusions

In summarizing this work, I would like to make the following points:

1. A detailed evaluation of the photon noise contribution to the fluctuations of the observed position of the 1548 line has confirmed that the previously observed rise in rms velocity with decreasing intensity is largely due to photon statistics. After correction for photon noise, the best estimate of the average (rms) velocity is in the range 1-2 km/sec, rather than the 3 km/sec value reported earlier by Bruner (1978) and by Athay and White (1979). The average value refers to a field of view of  $1 \times 20$  arc sec which will usually contain multiple emission elements that may move with independent phase (Bartoe and Brueckner, 1975; Brueckner, 1979). This value is appropriate for both active and quiet regions.

2. A consistency test comparing the expected level of rms velocity for a given intensity modulation showed that the observed fluctuations are consistent with the presence of acoustic waves.

3. A propagation test incorporating the cross correlation between intensity and velocity fluctuations has been introduced to determine whether observed motions correspond to propagating waves. Examples of both propagating and evanescent waves are found in the data, as well as regions that were quiescent at the time of observation.

4. Application of the cross correlation test revealed both upward and downward propagating waves with about equal frequency. On the average, the upward and downward fluxes tend to cancel such that the net acoustic flux density is statistically indistinguishable from zero.

5. The upper limit to the acoustic flux available for coronal heating, based on the statistics of the flux measurement, is three orders of magnitude too low to heat the corona. Although this limit may be too severe because of the neglect of multiple emission elements, it appears to be extremely unlikely that the required energy could have been masked by this effect.

## Acknowledgements

I am pleased to acknowledge the contributions of the OSO-8 Team at the University of Colorado in the collection of these data. Particular thanks go

to Ms. Celia Chisholm who did much of the compilation of the data files that entered the analysis. A number of utility computer programs developed by R.A. Shine were also quite useful. The analysis and its presentation have undoubtedly been improved through a number of helpful conversations with J.W. Leibacher. This work was supported under NASA Contract NAS5-22411.

## References

- Athay R.G., 1976, "The Solar Chromosphere and Corona: Quiet Sun," (Dordrecht: Reidel).
- Athay, R.G., and White, O.R., 1978, *Astrophys. J.*, 226, 1135.
- Athay, R.G., and White, O.R., 1979, *Astrophys. J.*, 229, 1147
- Bartoe, J., and Brueckner, G, 1975, *Bull. A.A.S.*, 7, 432.
- Brueckner, G., 1979 (private communication).
- Bruner, E.C., Jr., 1977, *Space Sci. Instrum.*, 3, 369.
- Bruner, E.C., Jr., 1978, *Astrophys. J.*, 226, 1140.
- Bruner, E.C., Jr., and Lites, B.W., *Astrophys. J.*, 228, 322.
- Bruner, E.C., Jr., and McWhirter, R.W.P., *Astrophys. J.*, 231, 557.
- Dahlquist, G., and Bjork, A., 1974, "Numerical Methods" (Prentice-Hall).
- Haisch, B., and Linsky, J., 1976, *Astrophys. J.*, 205, L39.
- Hansen, E.R., and Bruner, E., 1979, *Space Sci. Instrum.*, in press.
- Lamb, H., 1945, "Hydrodynamics" (Dover).
- Lites, B.W., and Hansen, E.R., 1978, *Solar Physics*, 55, 347.
- Noyes, R.W. and Leighton, R., 1963, *Astrophys. J.*, 138, 631.
- Rottman, G.J., 1976, (private communication).
- Withbroe, G., and Noyes, R.W., 1977, *Ann. Rev. Astr. Ap.*, 15, 363.

## Figure Captions

Figure 1. Spurious velocity signals introduced by photon counting statistics. The diamonds are the results from a Monte Carlo simulation; the smooth curve is the adopted noise function used in correcting the experimental data. This curve is applicable to data set 1.

Figure 2. Predicted spurious velocity signal (solid line) compared with observations of Data Set 1 (triangles). It is seen that much of the observed velocity signal at low intensity levels is due to the effect of photon counting statistics.

Figure 3. Data Set 1 after correction for photon noise.

Figure 4. Data Set 2. Spurious velocity predictions compared to observations.

Figure 5. Data Set 2 after correction for photon noise. Observations falling below the predicted noise level are reported with zero velocity.

Figure 6. Consistency test for the presence of acoustic waves. Observed rms velocities from Data Set 1 are plotted against observed values of rms intensity modulation. The circles correspond to quiet region observations and the squares to active regions. The curves show the predicted relationship between rms velocity and intensity modulation if the disturbances are due to acoustic waves. The curves should define the upper boundary of an observed distribution, since the direction of waves propagation will not, in general, be along the line of sight.

Figure 7. Acoustic Flux Densities computed from the observations of Data Set 1.

Figure 8. Acoustic Flux Densities computed from the observations of Data Set 2.

Fig. 2

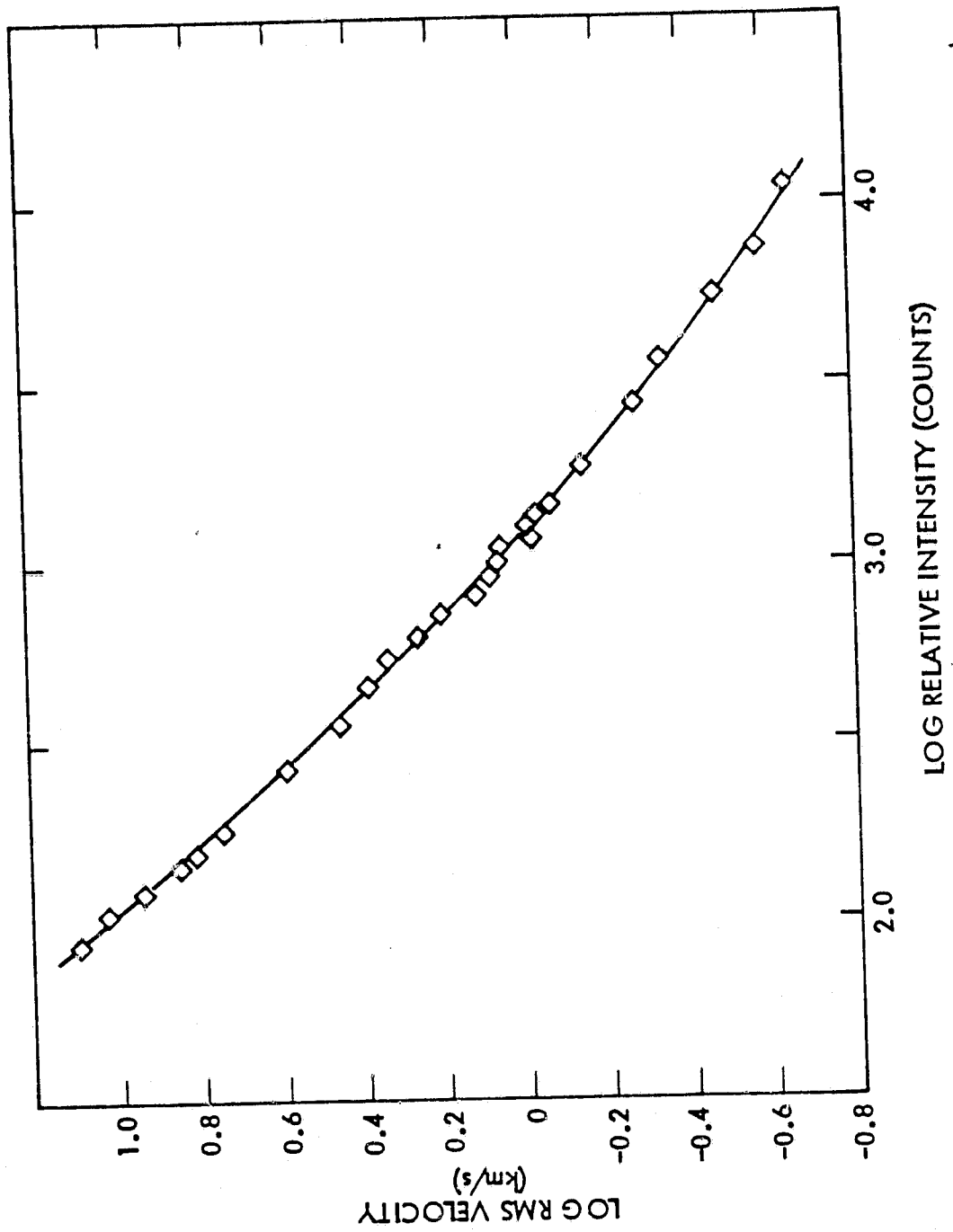
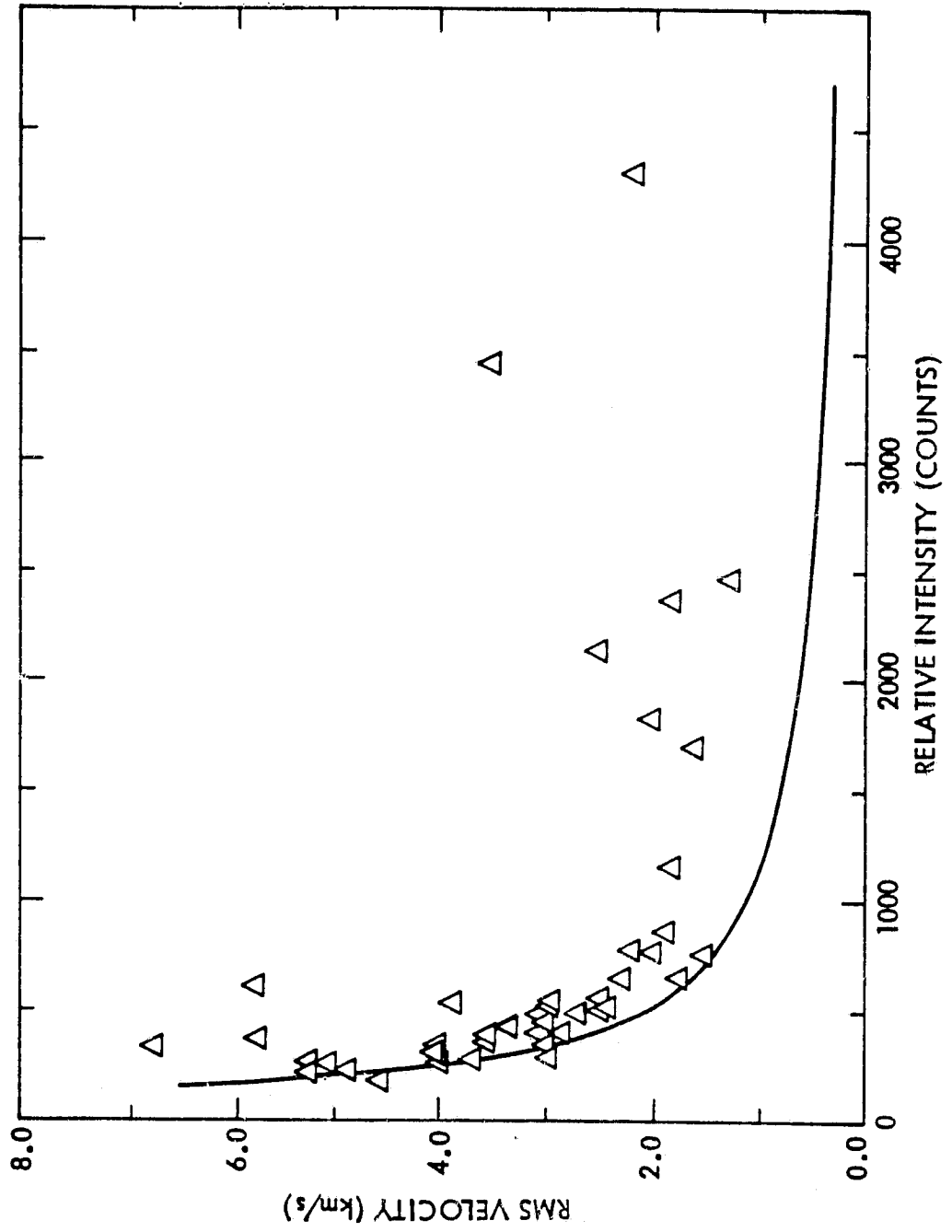
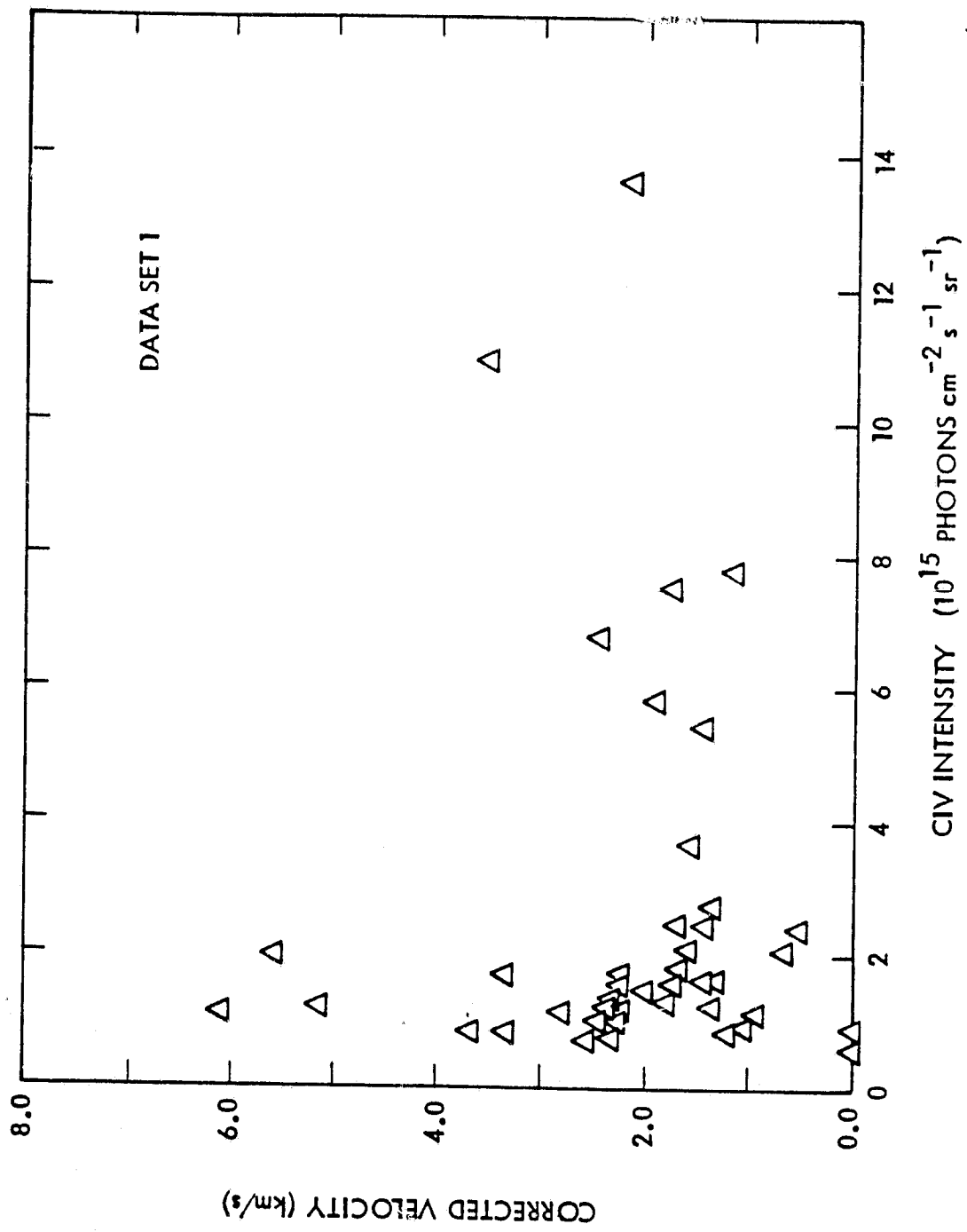
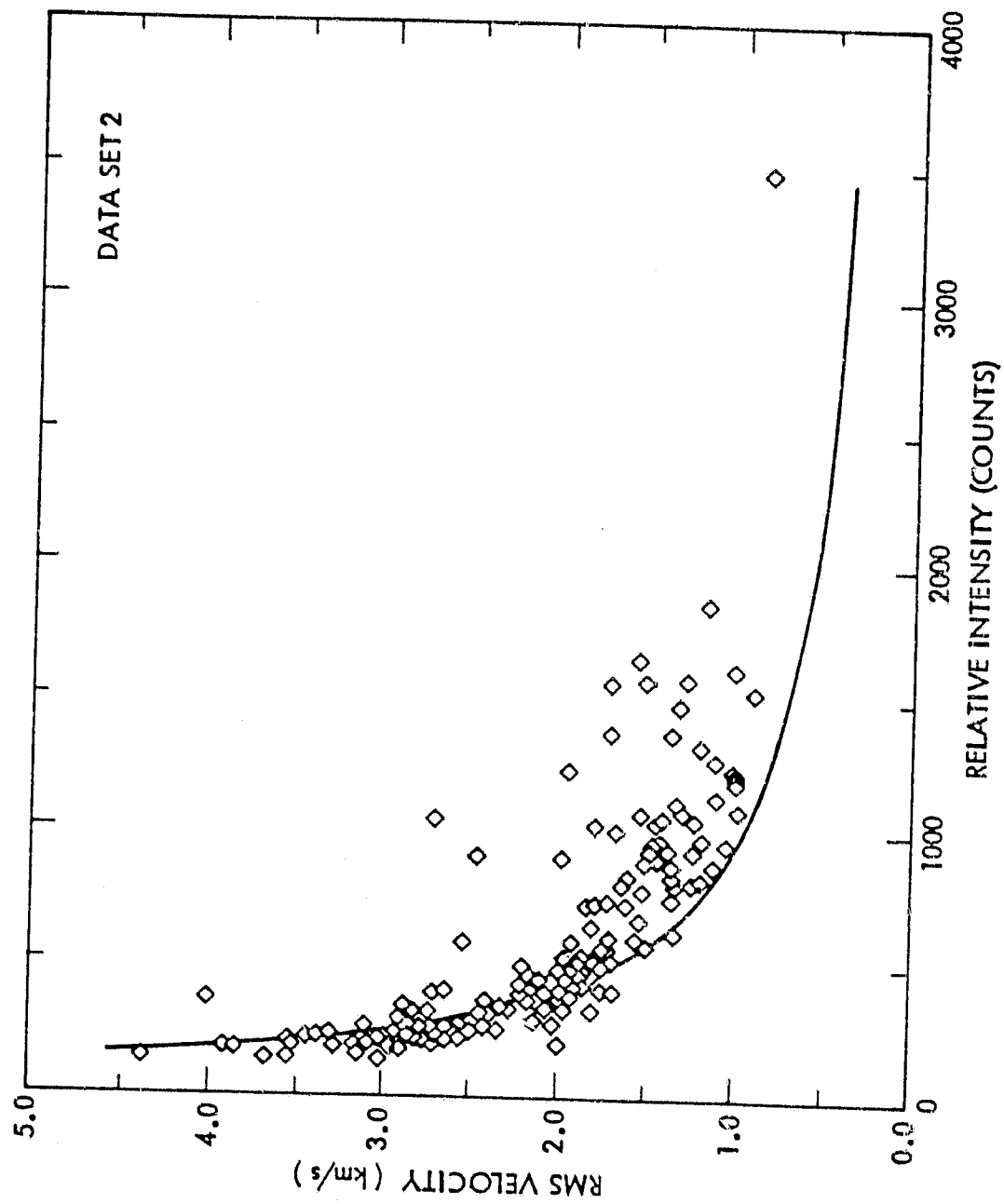


Fig. 2.







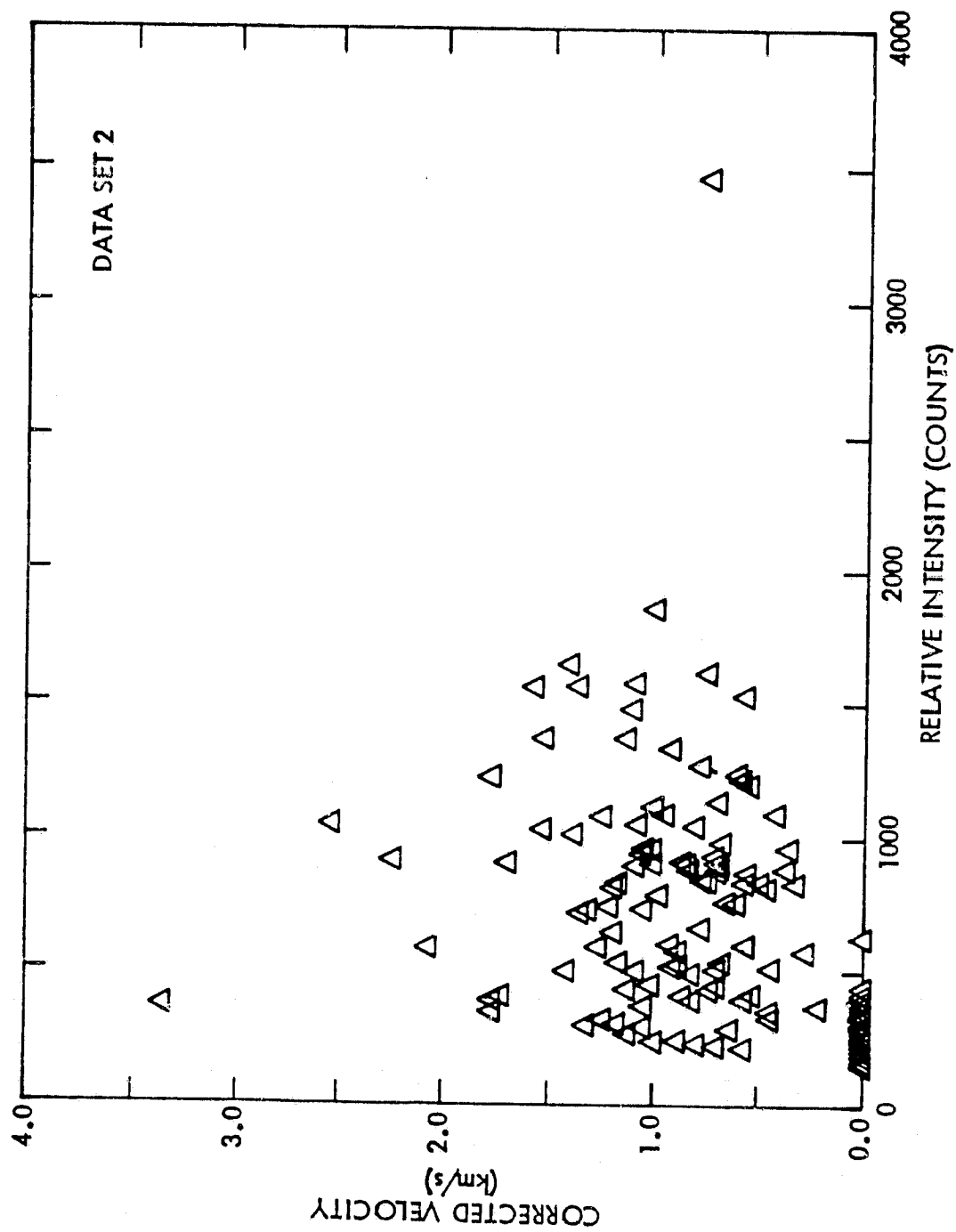


FIG. 6

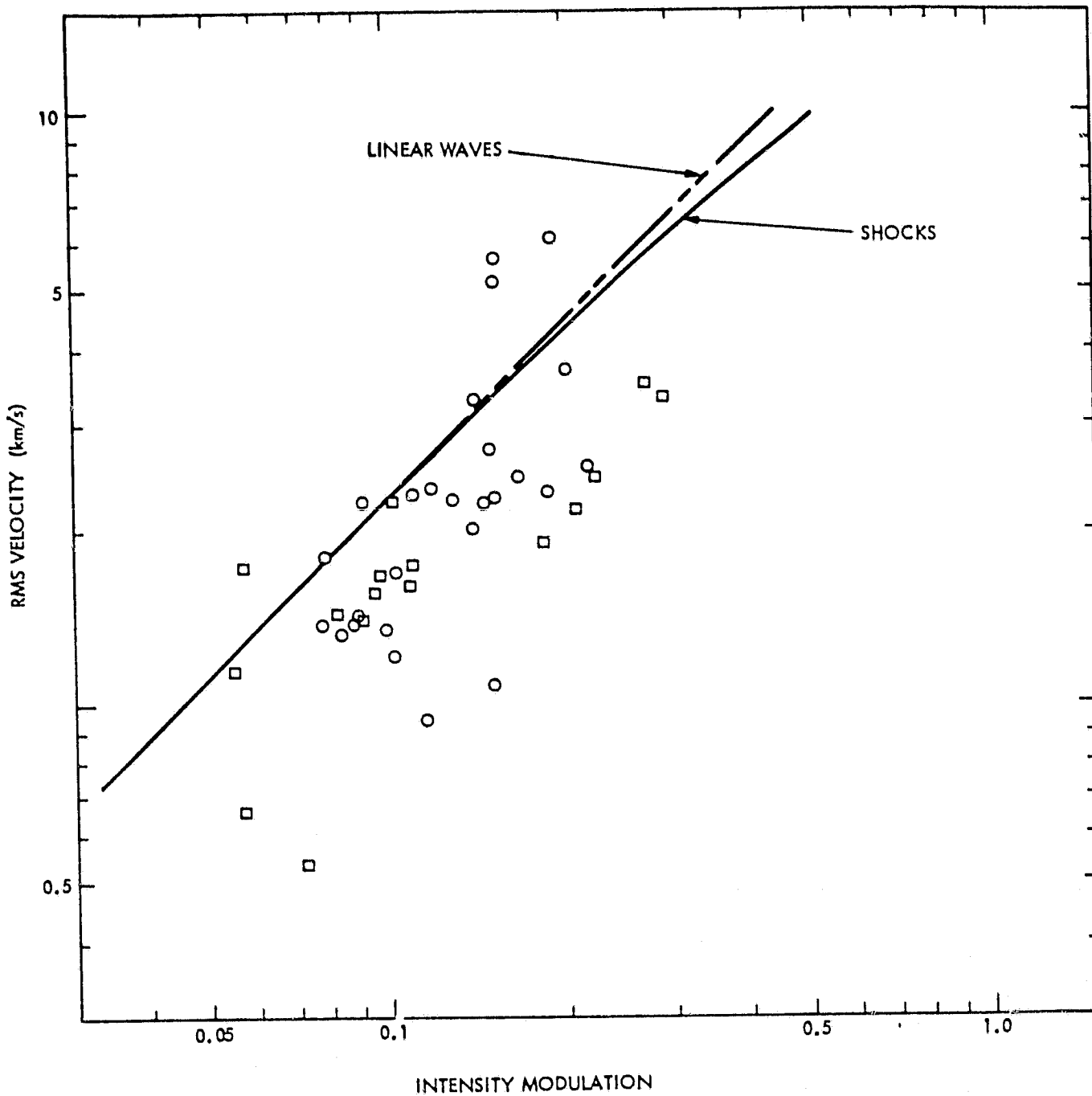


Fig. 7

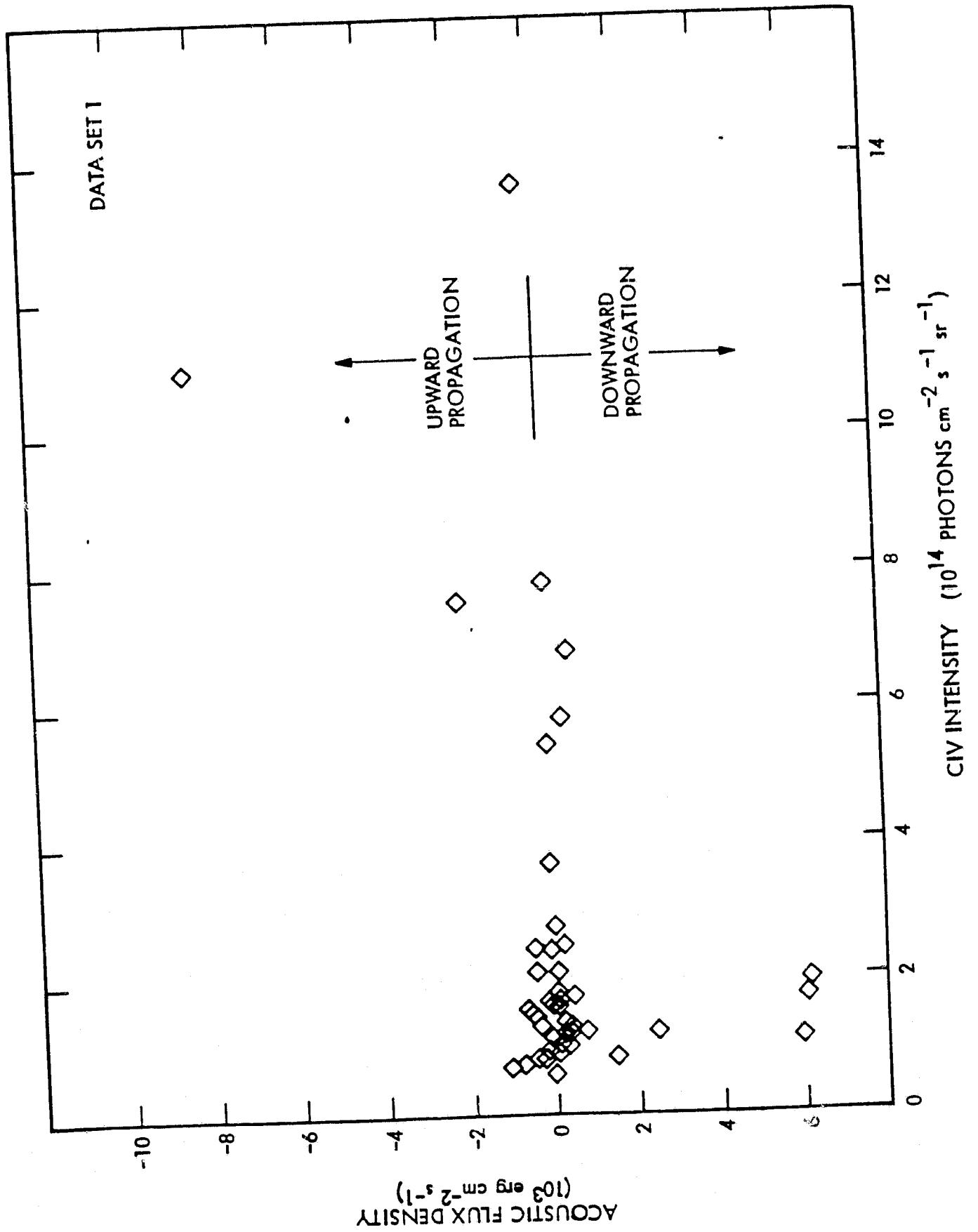


FIG. 6\*

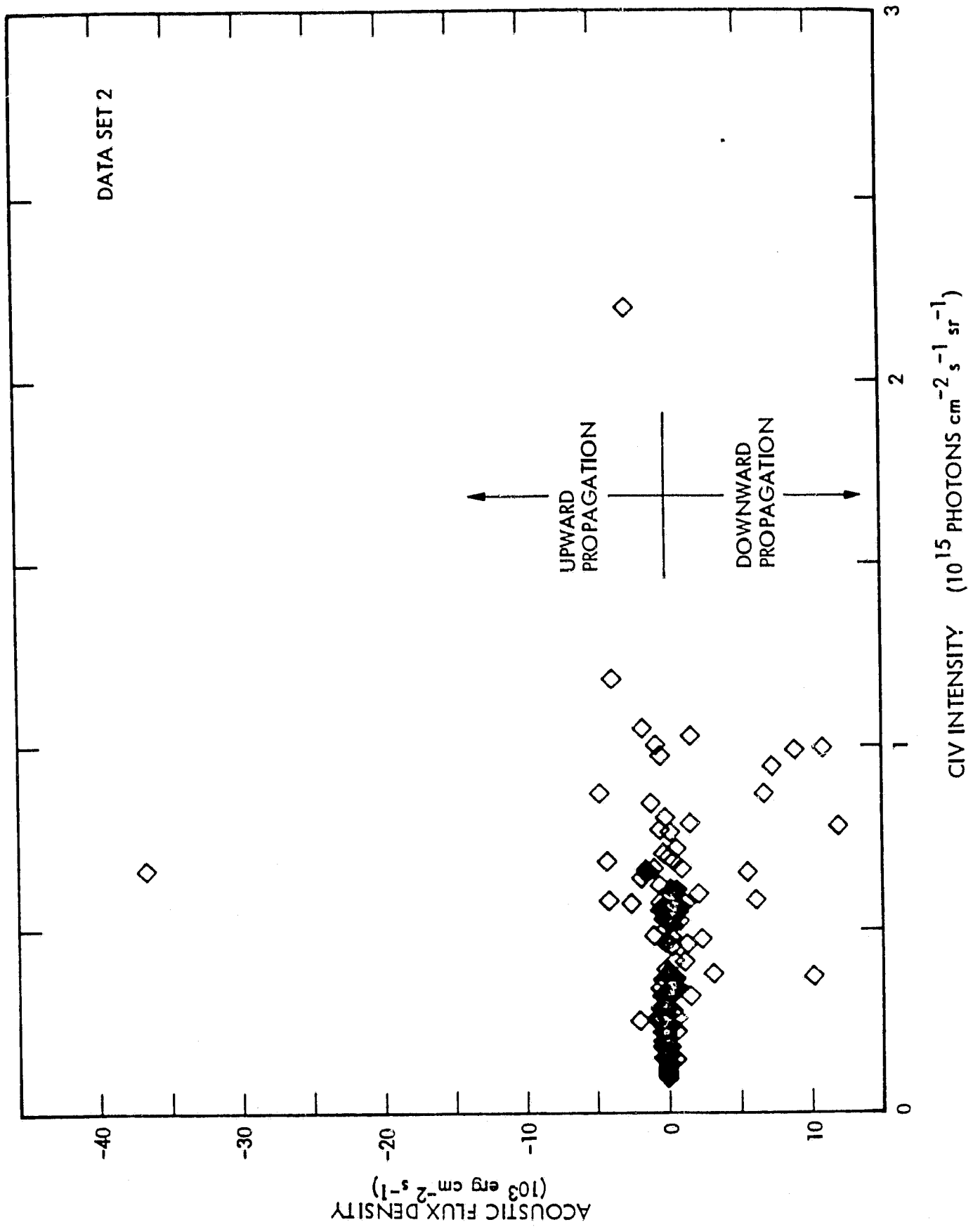


TABLE 1

	C IV Intensity Photons $\text{cm}^{-2} \text{sec}^{-1} \text{ster}^{-1}$	Intensity Modulation	RMS Velocity $\text{km sec}^{-1}$	Cross Correlation	Acoustic Flux Density $\text{erg cm}^{-2} \text{sec}^{-1}$		
QUIET REGIONS	A05176	$1.47 \times 10^{14}$	.140	2.02	-.127	-513	
	A05185	2.74	.077	1.79	.053	81	
	A05191	1.67	.091	2.23	-.040	-116	
	A07322	0.84	.200	3.67	-.038	-398	
	A08047	1.34	.110	2.32	.087	317	
	A08050	1.22	.088	1.78	.191	331	
	A08051	0.75	.186	2.33	-.112	-693	
	A08052	1.30	.078	1.79	.215	429	
	A04041	1.94	.152	5.57	.511	6180	
	A03759	1.17	.130	2.25	.091	380	
	A04157	1.09	.190	6.09	.757	5900	
	A03647	1.61	.089	1.43	.062	113	
	A05151	0.69	.218	2.55	-.128	-1016	
	A03762	1.61	.083	1.34	-.020	-32	
	A03649	1.12	.116	0.94	-.025	-39	
	A03826	1.54	.146	2.24	-.129	-603	
	A09190	0.98	.152	2.27	-.026	-128	
	A05142	0.90	.150	1.07	.034	78	
	A03791	1.00	.165	2.46	.056	325	
	A04039	1.11	.148	2.80	.051	302	
	A04071	1.19	.152	5.12	.223	2480	
	A10920	0.60	.110	0.0	.115	-	
	A05170	1.28	.099	1.75	-.157	-300	
	A05203	2.46	.103	1.70	.122	30	
	A07324	1.22	.119	2.37	.190	766	
	A10919	0.92	.086	0.0	-.113	-	
	A05157	0.83	.141	3.30	.225	1500	
	A05163	0.84	.101	1.22	-.171	-301	
	ACTIVE REGIONS	A09831	$1.70 \times 10^{14}$	.289	3.33	.440	$60.5 \times 10^3$
		A08720	2.42	.090	1.43	-.212	-3.9
		A09357	1.80	.097	1.67	.376	8.7
		A06390	7.49	.110	1.74	-.721	-19.7
		A05658	3.66	.095	1.56	.007	0.15
A04514		7.76	.055	1.15	.060	0.54	
A06301		2.07	.057	.65	.241	1.3	
A04519		13.5	.207	2.17	-.054	-3.5	
A03662		5.76	.182	1.91	.080	4.0	
A03651		6.74	.222	2.45	.007	0.54	
A10174		1.57	.057	1.75	.019	0.26	
A05596		2.06	.109	1.60	-.155	-0.39	
A06237		1.09	.269	3.51	-.614	-82.8	
A06299		1.73	.101	2.25	.160	5.2	
A06322		2.39	.072	.54	.019	0.11	
A06303		5.38	.082	1.45	.012	0.20	

ORIGINAL PAGE IS  
OF POOR QUALITY

## BIBLIOGRAPHY

NOTE: For publications produced under this contract, please see Appendix A.

- Acton, L.W., Wolfson, C.J., Datlowe, D.W., Mosher, J.M., Roethig, D.T., and Smith, K.L. (1980): "The Lockheed OSO-8 Program: Analysis of Data from the Mapping X-Ray Heliometer Experiment," NASA GSFC Final Report (NAS5-22411, Task Ib).
- Bruner, E.C., Jr., (1977): The University of Colorado OSO-8 Spectrometer Experiment, I: Introduction and Optical Design Considerations," Space Science Instrumentation 3, 369.
- Bruner, E.C., Jr. (1978): "Dynamics of the Solar Transition Zone," The Astrophysical Journal 226, 1140.
- Bruner, E.C., Jr., and Lites, B.W. (1979): "Mass Motions in Impulsive Flarelike Brightenings as Observed by OSO-8," The Astrophysical Journal 228, 322.
- Hansen, E.R. and Bruner, E.C., Jr. (1979): "The University of Colorado OSO-8 Spectrometer Experiment, IV: Missions Operations," Space Science Instrumentation 5, 3.
- Stern, D.M. and Klemp, M. (1976): "SOL: The OSO Data Reduction Language," Laboratory for Atmospheric and Space Physics, University of Colorado, Boulder, Colorado 80309.
- University of Colorado (1975): OSO-I User Handbook - CU/LASP Experiment, Volumes 1, 2, and 3, Laboratory for Atmospheric and Space Physics, University of Colorado, Boulder, Colorado 80309.
- University of Colorado (1977): OSO-I HRUV Spectrometer Operations Manual, Laboratory for Atmospheric and Space Physics, University of Colorado, Boulder, Colorado 80309.
- Wolfson, C.J., Acton, L.W., and Smith, K.L. (1978): "Final Report for the Orbital Operations Portions of the Mapping X-Ray Heliometer Program (OSO-8)", NASA GSFC Final Report (NAS5-22411, Task Ia).

Index

	Page
Acoustic Energy Flux.....	6
Cataloging.....	2
Computer programs.....	2
Data Available.....	1
Data Processed.....	4
Distribution of Data.....	4
Flares.....	5
New Technology.....	6
Preprints.....	8, 47
Publications.....	7
References.....	7, 73
Results.....	4
Short-Lived Brightenings.....	5